nature microbiology

Article

https://doi.org/10.1038/s41564-026-02277-8

Bacterial Schlafen proteins mediate phage defence

Received: 10 July 2025

Accepted: 26 January 2026

Published online: 09 March 2026

Check for updates

Veronica Perez Taboada[1], Yimo Wu[1], Riley Cassidy[1], Kirill E. Medvedev[2], Luuk Loeff[3], Anna Nemudraia[1] ✉ & Artem Nemudryi[1,4] ✉

Human Schlafen proteins restrict viral replication by cleaving tRNA, thereby suppressing protein synthesis. Although the ribonuclease domain of Schlafen proteins is conserved across all domains of life, its function in prokaryotes has remained unclear. Here we demonstrate that prokaryotic Schlafen nucleases are widespread antiviral effectors that protect bacteria from bacteriophages and are fused to a diverse array of phage-sensing domains. We expressed seven Enterobacterales Schlafen systems in *Escherichia coli*, identifying two that confer defence against coliphages. We focused on a system where Schlafen nuclease is fused to a previously unknown immunoglobulin-like sensor domain and demonstrated that it recognizes tail assembly chaperones of T5-like phages. Upon activation, the Schlafen nuclease cleaves both *E. coli* and phage-encoded tRNAs and restricts T5 phage by reducing its burst size. Our findings redefine Schlafens as an ancient, mechanistically conserved family of immune effectors, revealing the deep evolutionary origin of tRNA-targeting antiviral immunity in humans.

The mammalian Schlafen (Slfn) protein family was identified in 1998 and named for its ability to induce growth arrest in murine thymocytes ('Schlafen' is German for 'sleep')[1]. Later work found that mammalian Slfn proteins share a conserved N-terminal endoribonuclease domain that suppresses protein synthesis by cleaving transfer RNA (tRNA) and rRNA[2–6] and that several Slfn members act as interferon-inducible antiviral factors[7,8]. In particular, human SLFN11 restricts diverse viruses, including human immunodeficiency virus 1 (ref. 5), human cytomegalovirus[9] and positive-strand RNA flaviviruses, such as Zika and Dengue viruses[10]. Human sterile alpha motif domain-containing protein 9 (SAMD9) and its paralogue, SAMD9-like protein (SAMD9L), similarly use an Slfn-like tRNase domain to inhibit translation during poxviral and lentiviral infections[11,12].

The Slfn ribonuclease domain is highly conserved in animals and, in addition to antiviral defence, has been linked to suppressing transposable elements in roundworms[13]. This recurring recruitment of the Slfn ribonuclease domain for immune functions suggests deep evolutionary roots of its role in restricting genetic parasites[8,13,14]. Slfn domains are found in prokaryotic genomes and a few instances have been reported to associate with anti-phage genes, hinting at a potential immune function[15–18]. However, direct experimental evidence for the antiviral role of prokaryotic Schlafens (pSlfns) has been lacking and their molecular mechanisms remained unknown.

Here, we use a combination of computational, functional and biochemical assays to demonstrate that pSlfn domains are anti-phage effectors fused to a variety of potential phage sensors. We then determine the molecular mechanism of phage defence mediated by pSlfn nuclease fused to an immunoglobulin-like domain. We show that pSlfn-mediated tRNA cleavage triggers growth arrest in response to phage infection, revealing evolutionary, functional and mechanistic conservation with human Slfn-mediated antiviral immunity.

Results

Bacterial Schlafen proteins mediate phage defence

The human SLFN11 protein has an N-terminal ribonuclease (RNase) domain, a linker domain and a C-terminal DNA/RNA helicase domain[4].

[1]Department of Biochemistry and Molecular Biology, College of Medicine, University of Florida, Gainesville, FL, USA. [2]Department of Computer Science, University of Central Florida, Orlando, FL, USA. [3]Department of Cell and Chemical Biology, Leiden University Medical Center, Leiden, the Netherlands. [4]UF Genetics Institute, University of Florida, Gainesville, FL, USA. ✉e-mail: anemudraia@gmail.com; artem.nemudryi@gmail.com

https://doi.org/10.1038/s41564-026-02277-8

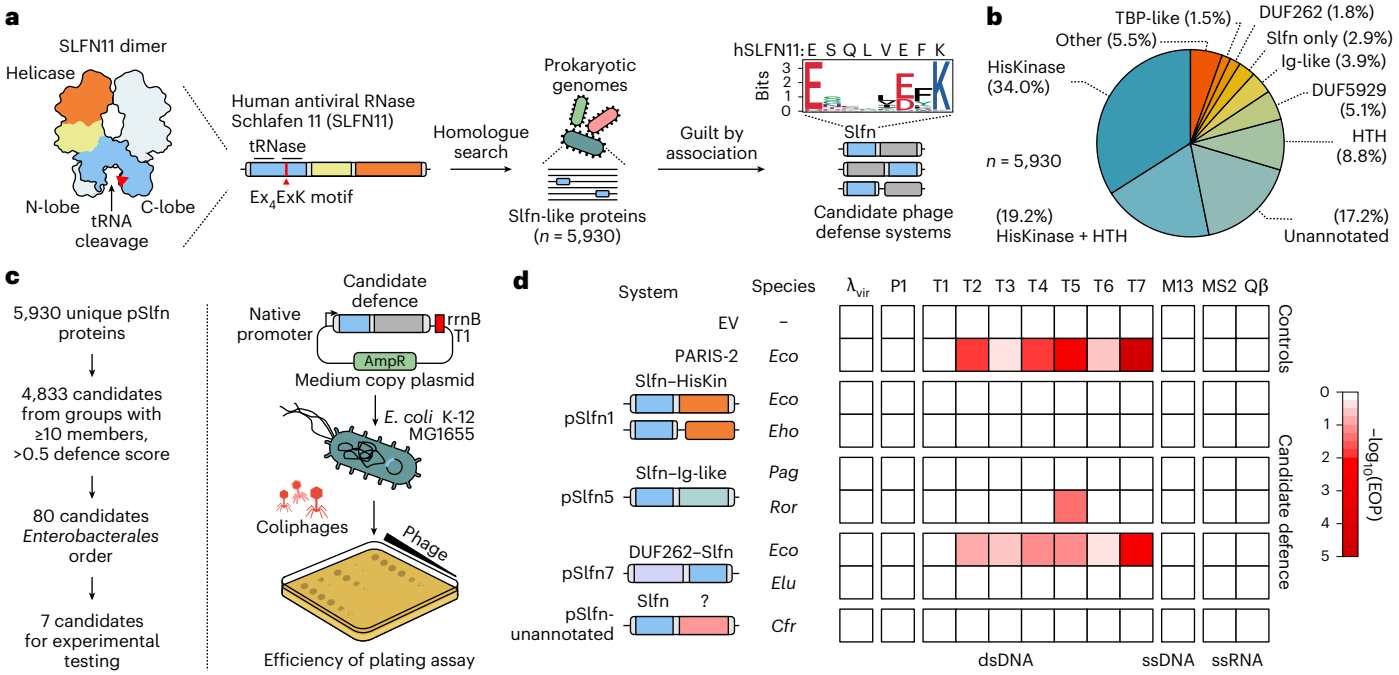

Fig. 1 | Schlafen proteins mediate phage defence. a, The computational approach to identify prokaryotic homologues of Schlafen nucleases (Slfn) with predicted roles in phage defence. This search found 5,930 unique Slfn protein sequences (100% CD-HIT cut off). The Weblogo plot shows the conserved Ex_4(E/D)xK motif in prokaryotic Slfn domains. **b**, Annotation of domains fused to Slfn in the 5,930 identified proteins. **c**, Experimental approach to test for immune activities of Slfn proteins. **d**, Immune activities of tested Slfn proteins (top to bottom) against a panel of phages that infect *E. coli* (left to right). *Cfr*, *Citrobacter freundii*; *Eco*, *Escherichia coli*; *Eho*, *Enterobacter hormaechei*; *Elu*, *Enterobacter ludwigii*; *Pag*, *Pantoea agglomerans*; *Ror*, *Raoultella ornithinolytica*; dsDNA, double-stranded DNA; ssDNA, single-stranded DNA; ssRNA, single-stranded RNA; λ_{vir}, virulent mutant of phage λ.

The N-terminal domain consists of two lobes (N- and C-lobe), where the C-lobe contains the ribonuclease active site with a catalytic Ex_4ExK motif that is essential for tRNA cleavage[4] (Fig. 1a). To identify prokaryotic Slfn homologues, we searched for Slfn nuclease domains in reference prokaryotic genomes and identified 5,930 unique (9,937 total) protein sequences across 4 archaeal and 34 bacterial phyla (Fig. 1a, Extended Data Fig. 1a and Supplementary Table 1). Subsequent multiple sequence alignments show a highly conserved Ex_4(E/D)xK sequence motif in the predicted active site, which matches the catalytic residues of SLFN11, suggesting a conserved enzymatic mechanism (Fig. 1a and Extended Data Fig. 1b).

Prokaryotic defence genes frequently cluster in the host genome, forming genetic neighbourhoods known as defence islands[15,19]. To determine whether pSlfn proteins reside in defence islands, we performed a genetic neighbourhood analysis and found that 69.6% of identified pSlfn genes are located within a ±10-kb distance to at least one known defence gene (Extended Data Fig. 1a and Supplementary Table 1). On average, identified pSlfn genes co-localize with 1.9 defence genes, which is comparable to AriB (2.74), the nuclease effector of the phage anti-restriction-induced system (PARIS)[20,21], and approximately ten-fold higher than the housekeeping genes rpL3 (0.13) and L1p (0.19) (Extended Data Fig. 1c). This genetic association suggested that pSlfns may function in phage defence. Notably, 30.4% of identified pSlfn genes were not associated with defence genes, suggesting that in some instances, pSlfn domains may have non-immune functions or that these pSlfn genes are in defence hot spots that have not been annotated yet[21,22].

Phage defence systems often function through sensors that detect infection and effectors that execute the immune response. These functional modules can be encoded within a single gene or split across multiple genes[23,24]. We found that 97.1% of identified pSlfn domains are fused to other protein domains, where pSlfns most probably act as effectors, while the identified fused domains may function as sensors (Fig. 1b). To classify the diversity of domain architectures among pSlfn proteins, we used a combination of sequence and structural homology-based computational methods, identifying 55 distinct domain compositions, which we designated pSlfn1 through pSlfn55 (Supplementary Table 2). The most frequent domain compositions include fusions of pSlfn to histidine kinase (HisKinase, 34.0%), HisKinase and helix-turn-helix domains (HisKinase–HTH, 19.2%), HTH domains (8.8%), DUF5929 (5.1%), domains with immunoglobulin-like fold (Ig-like, 3.9%), DUF262 (1.8%) and TBP-like domains (1.5%) (Fig. 1b). Of 5,930 identified pSlfns, 1,020 (17.2%) are fused to protein domains that show no substantial homology to the domains annotated in the Pfam and Evolutionary Classification of protein Domains (ECOD) databases[25,26]. We further grouped these proteins into 558 sequence similarity clusters (Supplementary Table 2). This diversity of domain compositions in pSlfn proteins probably represents combinations of the core Slfn effector module with various sensors that respond to different cues and regulate its nuclease activity.

To test whether pSlfn genes confer phage defence, we focused on four domain architectures found in Enterobacterales, comprising fusions with HisKinase, Ig-like, DUF262 and unannotated domains. We manually picked two systems from each group, prioritizing those with the most neighbouring defence genes and greatest amino acid sequence divergence (Extended Data Fig. 1d and Supplementary Table 3). One construct failed during synthesis, leaving seven systems. We expressed these in the *E. coli* K-12 strain MG1655 under their native promoters and challenged the cells with a panel of diverse *E. coli* phages (Fig. 1c,d and Supplementary Table 4). As a positive control, we used a plasmid encoding the *E. coli* B185 PARIS-2 immune system[21], while an empty vector (EV) served as a negative control. In the tested subset, two pSlfn genes provided defence against T phages (Fig. 1d and Extended Data Fig. 1e,f). We found that the DUF262–Slfn fusion from

https://doi.org/10.1038/s41564-026-02277-8

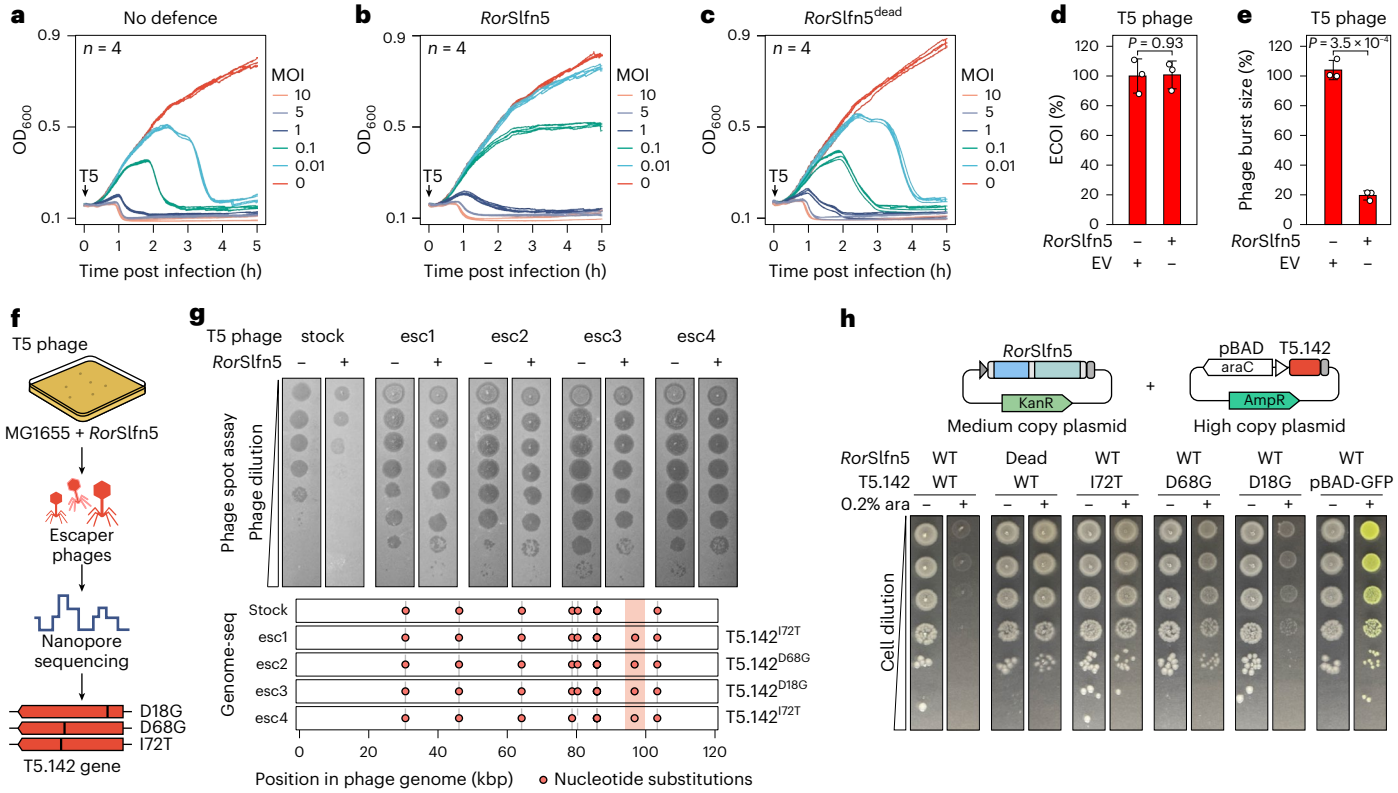

Fig. 2 | Phage tail assembly chaperone triggers pSlfn5-mediated phage defence. a–**c**, The growth kinetics of *E. coli* K-12 MG1655 cells without the defence (**a**), with *Ror*Slfn5 (**b**) or the nuclease-dead *Ror*Slfn5$^{E15A, D20A}$ mutant (**c**) following T5 bacteriophage infection at various MOIs. Each line shows a biological replicate ($n = 4$). **d**,**e**, The ECOI (**d**) and average burst size (**e**) of T5 phage in *Ror*Slfn5-expressing *E. coli* MG1655 cells compared with the EV control. The data are shown as the mean of three biological replicates ± s.d. A two-sided Welch's *t*-test was used to compare the experimental and control groups. **f**, An experimental approach to identify viral triggers of *Ror*Slfn5. **g**, Top: plaque assays with *Ror*Slfn5-escaping T5 phages (esc1–esc4). Bottom: mapping of mutations in T5 phage escapers compared with a reference phage genome. The vertical lines indicate mutations found in the laboratory T5 phage stock compared with the reference NCBI sequence. Vertical orange box highlights mutations present in escaper phages but not in the original viral stock. **h**, A toxicity assay in MG1655 cells co-transformed with the *Ror*Slfn5 plasmid and a plasmid for arabinose-inducible expression of T5.142 protein. Tenfold serial dilutions were spotted on agar plates with 0.2% glucose (−) or 0.2% arabinose (ara) (+). pBAD-GFP was used as a control for arabinose-dependent induction.

E. coli UC4224 (*Eco*Slfn7) significantly reduced the efficiency of plating (EOP) of a broad range of phages, with the most robust activity against the T7 phage (538.5 ± 194.4-fold EOP reduction, $P = 6.9 \times 10^{-4}$). By contrast, the Slfn fusion with Ig-like domain from *Raoultella ornithinolytica* (*Ror*Slfn5) protected *E. coli* only against T5 phage, reducing the EOP by 22.3 ± 1.0-fold ($P = 3.0 \times 10^{-11}$) (Extended Data Fig. 1f). Overall, these data demonstrate that prokaryotic Schlafen proteins protect bacteria from phage infection and exhibit distinct phage specificities that are probably determined by their fused domains.

RorSlfn5 reduces the productivity of the T5 phage

To elucidate the mechanisms that underpin the immune function of pSlfn proteins, we focused on *Ror*Slfn5 defence, which features an uncharacterized Ig-like domain, suggesting a mode of phage sensing that was not previously described. We challenged MG1655 cells with T5 phage at different multiplicities of infection (MOIs) and monitored cell growth over time. At low MOIs (0.01 and 0.1), cells expressing *Ror*Slfn5 survived the infection compared with cells without the defence system, whereas infections at high MOIs (5 and 10) resulted in all cultures collapsing approximately 60 min post infection, which agrees with the reported lysis time for T5 phage[27] (Fig. 2a,b). Further, at a MOI of 10, the phage titre in supernatants of *Ror*Slfn5-expressing cells at 60 min post infection was reduced by 59.3 ± 8.6% compared with the no defence control ($P = 7.6 \times 10^{-3}$; Extended Data Fig. 2a). Alanine substitutions in the catalytic Ex_4DxK motif (E15A, D20A) of the Slfn domain abolished defence at low MOIs and rescued phage titre at a high MOI, indicating that the nuclease activity of *Ror*Slfn5 is required for the phage defence (Fig. 2c and Extended Data Fig. 2a).

The collapse of *Ror*Slfn5-expressing cultures at high MOIs and reduced phage titres suggested that the phage defence may act by triggering abortive infection, killing the host cell before phage replication is completed[28,29]. To test this hypothesis, we performed the efficiency of centre of infection (ECOI) assay, which quantifies the number of productive infections that release at least one infectious progeny phage[30]. However, we found no significant difference in the number of infective centres between *Ror*Slfn5-expressing cells and the EV control, indicating that *Ror*Slfn5 does not abort T5 phage infection ($P = 0.94$; Fig. 2d). Reduced EOP (Fig. 1d) and lower phage titres with no changes in ECOI suggest that *Ror*Slfn5 reduces T5 phage productivity without completely eliminating the phage[31]. Consistent with this, the average burst size of T5 was reduced by 81.2 ± 3.0% in *Ror*Slfn5-expressing cells compared with the control ($P = 3.5 \times 10^{-4}$; Fig. 2e). Taken together, these assays indicate that *Ror*Slfn5 restricts T5 phage through a non-abortive mechanism that acts downstream of infection, limiting infectious phage progeny.

T5 tail assembly chaperone triggers RorSlfn5 phage defence

To determine the viral trigger for the *Ror*Slfn5 defence, we isolated T5 phages that escaped the immunity and sequenced their genomes (Fig. 2f). Four viral clones that we sequenced contained three distinct missense mutations (that is, D18G, D68G and I72T) in the T5.142 gene, which encodes for the phage tail assembly chaperone (NCBI accession:

https://doi.org/10.1038/s41564-026-02277-8

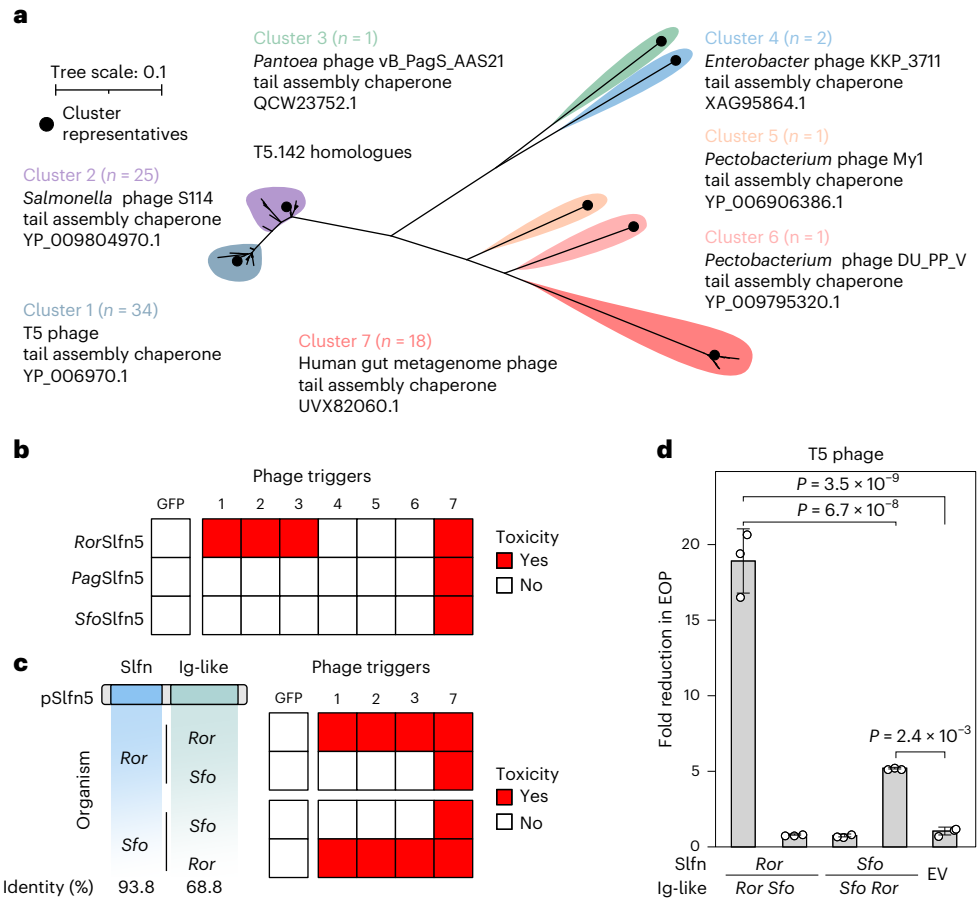

Fig. 3 | The Ig-like domain mediates the specificity of pSlfn5 immunity. **a**, A maximum-likelihood phylogenetic tree of T5.142 homologues. Selected representatives are listed for each homologue cluster and indicated with black dots. **b**, A summary of toxicity assays in MG1655 cells co-transformed with pSlfn5 (top to bottom) and T5.142 homologues from various phages (left to right) shown in Extended Data Fig. 2. The experiment was performed in three biological replicates and the results for one representative replicate are shown. The numbers correspond to the homologue clusters in **a**. **c**,**d**, Toxicity (**c**) and EOP assay (**d**) with chimeric pSlfn5 proteins with swapped Ig-like domains. The toxicity assays (Extended Data Fig. 4) were repeated independently three times with similar results. The data are shown for one replicate. EOP assay results are shown as mean ± s.d. of three biological replicates. The white dots show the average of three technical replicates for each biological replicate. A one-way ANOVA with post-hoc Tukey HSD test was used to compare the experimental groups. *Sfo*, *Serratia fonticola*.

YP_006970.1)[32] (Fig. 2g and Supplementary Table 5). To test whether the T5.142 protein triggers *Ror*Slfn5 defence, we cloned the viral gene and its escape variants into high-copy plasmid vectors under the control of the arabinose-inducible promoter (pBAD; Fig. 2h). Expression of T5.142 in cells co-transformed with the *Ror*Slfn5 plasmid resulted in toxicity, demonstrating that this viral protein is sufficient to trigger the defence. By contrast, cells expressing a catalytically inactive mutant of *Ror*Slfn5 (*Ror*Slfn5$^{E15A, D20A}$) showed no growth defect compared with uninduced cells, indicating that the toxicity is mediated by the T5.142-triggered nuclease activity of *Ror*Slfn5. In addition, escape mutations in the viral T5.142 protein rescued toxicity. Notably, while the T5.142^{D18G} variant reduced toxicity, it did not completely abolish it, suggesting that, in our experimental set up, it is less effective at evading *Ror*Slfn5 defence than D68G and I72T mutations.

The immunoglobulin-like domain of pSlfn5 is a phage sensor

Homologues of pSlfn5 from *Pantoea agglomerans* (*Pag*Slfn5; 39.6% sequence identity to *Ror*Slfn5) and *Serratia fonticola* (*Sfo*Slfn5; 79.6% sequence identity to *Ror*Slfn5) did not protect *E. coli* from T5 phage or any other phage tested (Extended Data Figs. 1f and 2b). The sequence divergence between these proteins is primarily driven by their C-terminal domains, while the N-terminal Slfn nuclease domains are more conserved (Extended Data Fig. 3a). The AlphaFold-predicted structure of *Ror*Slfn5 suggests that its C-terminal domain has an Ig-like β-sandwich fold with structural similarity to human integrin ectodomains (Extended Data Fig. 3b,c and Supplementary Table 6). These observations led us to hypothesize that the Ig-like domains of pSlfn5 proteins function as sensor modules that recognize viral proteins, and thereby *Pag*Slfn5 and *Sfo*Slfn5 might recognize T5.142 homologues from other phages.

To test this, we synthesized genes encoding six representative homologues of the T5 phage tail assembly chaperone (Fig. 3a). In addition to T5.142, *RorSlfn5* was triggered by expression of homologues from *Salmonella* phage S114, *Pantoea* phage vB_PagS_AAS21 and an unclassified phage from a human gut metagenome (Fig. 3b and Extended Data Fig. 2c). Consistent with the lack of defence against the T5 phage, *Pag*Slfn5 and *Sfo*Slfn5 were not activated by expression of T5.142, while the tail assembly chaperone from the human gut metagenome triggered all tested pSlfn5 homologues (Fig. 3b and Extended Data Fig. 2d,e). None of the identified triggers caused toxicity when expressed alone or co-expressed with a nuclease-dead *Ror*Slfn5$^{E15A, D20A}$ mutant, confirming that toxicity is mediated by the nuclease activity of pSlfn5 (Extended Data Fig. 2f,g). Together, these findings demonstrate that pSlfn5 proteins recognize tail assembly chaperones from phages in the *Demerecviridae* family, with different pSlfn5 homologues exhibiting distinct trigger specificities.

https://doi.org/10.1038/s41564-026-02277-8

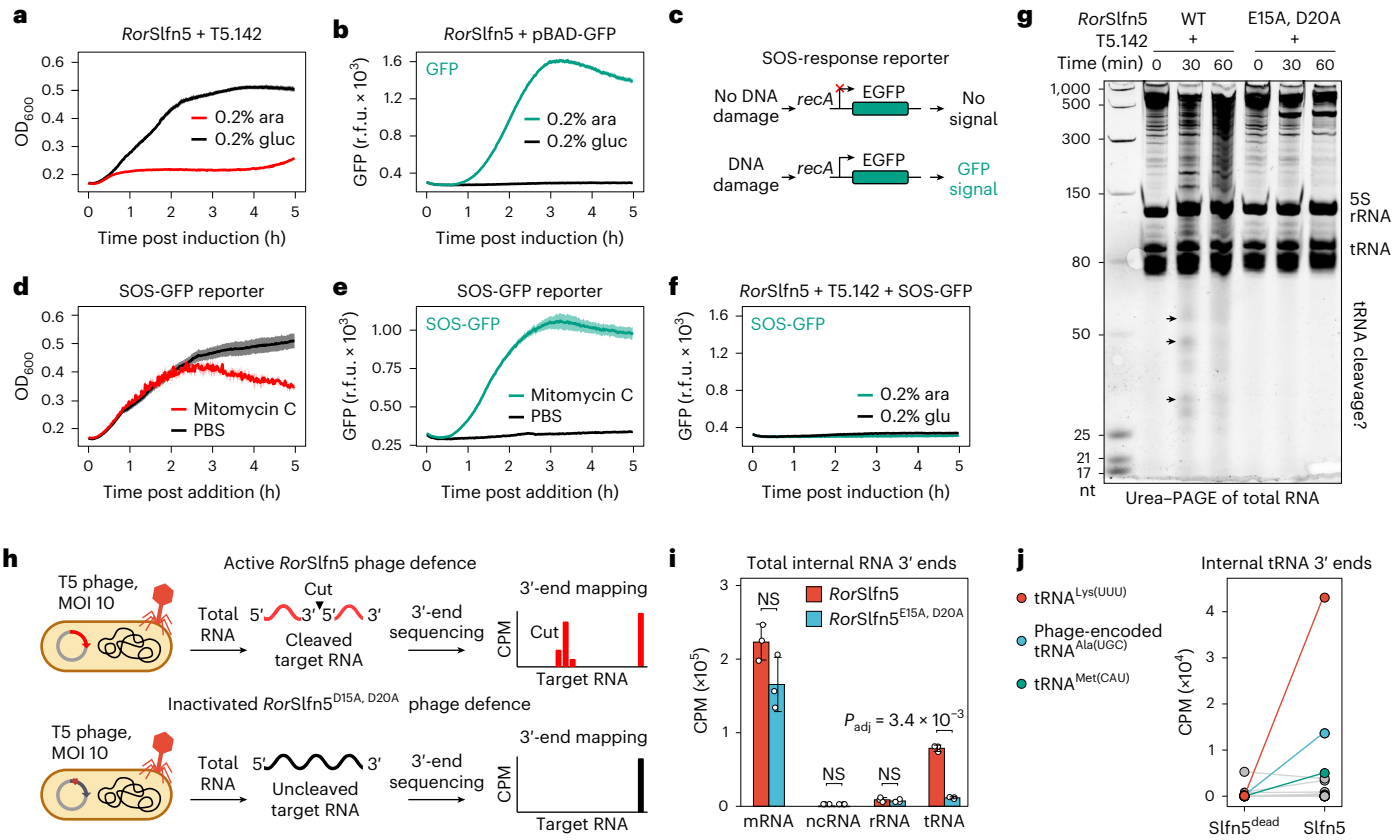

Fig. 4 | *Ror*Slfn5 cleaves tRNA upon phage infection. a, Growth kinetics of MG1655 cells constitutively expressing *Ror*Slfn5 with (0.2% arabinose (ara)) and without (0.2% glucose (gluc)) induction of T5.142 expression. **b**, Kinetics of GFP expression after induction of the pBAD promoter with arabinose. **c**, Schematics of the reporter assay for detecting SOS response upon DNA damage. **d**,**e**, Growth kinetics (**d**) and SOS-response reporter assay (**e**) of MG1655 treated with 100 nM mitomycin C or PBS. **f**, SOS-response reporter assay with *Ror*Slfn5-expressing cells after induction of T5.142 expression. The kinetic assays in **a**–**f** were performed in four biological replicates. The data are shown as mean (centre line) ± s.d. (ribbon). **g**, Urea–PAGE of total RNA extracted from *Ror*Slfn5 or *Ror*Slfn$^{E15A, D20A}$-expressing MG1655 at various timepoints after induction of T5.142 expression. Black arrows highlight RNA cleavage fragments. **h**, Schematics of the 3′-end RNA-seq approach used to map *Ror*Slfn5-mediated RNA cleavage in T5 phage-infected cells. **i**, Total abundance of non-native (internal) 3′ ends in different RNA types in T5 phage-infected cells expressing *Ror*Slfn5 or its nuclease-dead version (E15A and D20A mutation). The data are shown as the mean of three biological replicates ± s.d. Means were compared using a two-sided Welch's *t*-test. The resulting *P* values were adjusted using the Holm method to account for multiple comparisons. **j**, The total abundance of internal 3′ ends in bacterial and viral tRNAs. The data are shown as the mean of three replicates.

To confirm the sensor function of Ig-like domains in pSlfn5 defence, we created chimeric proteins by swapping the Ig-like domains of *Ror*Slfn5 and *Sfo*Slfn5. Cellular toxicity assays showed that phage trigger specificity was transferred along with the sensor domain (Fig. 3c and Extended Data Fig. 4). Furthermore, the chimeric protein containing the nuclease domain of *Sfo*Slfn5 and the *Ror*Slfn5 sensor (Sfo–Ror chimera) gained protection against T5 phage, whereas changing the Ig-like domain of *Ror*Slfn5 for that of *Sfo*Slfn5 (Ror–Sfo chimera) abolished defence against T5 (Fig. 3d). Wild-type (WT) *Ror*Slfn5 reduced T5 phage EOP by 18.9 ± 2.1-fold ($P = 3.5 \times 10^{-9}$), while the Sfo–Ror chimera was ~3.6-fold less efficient and reduced EOP by 5.2 ± 0.1-fold ($P = 2.4 \times 10^{-3}$).

Overall, these results demonstrate that the Ig-like domain determines phage specificity, indicating that it functions as a sensor module within the pSlfn5 defence system. The acquired defence in the Sfo–Ror chimera shows that these domains are modular and can be exchanged between orthologues. However, the reduced phage defence of the chimera compared with *Ror*Slfn5 suggests that effective immunity requires co-evolution between sensor and effector domains.

RorSlfn5 is a phage-activated tRNase

After identifying the viral cue that triggers pSlfn5 defence, we then investigated its mechanism. Co-expression of *Ror*Slfn5 with its viral trigger led to growth arrest ~30 min after inducing T5.142 expression (Fig. 4a). This timing mirrors the kinetics of GFP expression under the same promoter, which became detectable 30 min post-induction (Fig. 4b). Control cells co-expressing *Ror*Slfn5 and GFP or *Ror*Slfn5$^{E15A, D20A}$ and T5.142 showed no growth arrest, demonstrating that it is mediated by T5.142-triggered nuclease activity of the pSlfn domain (Extended Data Fig. 5a,b).

To test whether *Ror*Slfn5 targets DNA, we assessed bacterial DNA damage following T5.142-triggered *Ror*Slfn5 nuclease activity. We used a fluorescent reporter plasmid (pSOS-GFP) that encoded a *gfp* gene under the control of a *recA* promoter, which is upregulated in the bacterial SOS response to DNA damage (Fig. 4c). Treatment of MG1655 with mitomycin C, a DNA-damaging agent, induced a strong fluorescent signal, which was absent in PBS-treated cells (Fig. 4d,e). By contrast, cells co-transformed with *Ror*Slfn5, T5.142 and pSOS-GFP did not show increased fluorescence, suggesting that *Ror*Slfn5 activation does not cause DNA damage and the SOS response (Fig. 4f and Extended Data Fig. 5c,d). These results indicate that *Ror*Slfn5 does not act on DNA and probably retains RNase activity as its primary mechanism of toxicity, consistent with the function of human SLFN proteins[3,4].

To test whether *Ror*Slfn5 targets RNA, we co-transformed MG1655 cells with plasmids encoding the T5.142 trigger and either WT *Ror*Slfn5 or a catalytically inactive mutant *Ror*Slfn5$^{E15A, D20A}$. We extracted total

https://doi.org/10.1038/s41564-026-02277-8

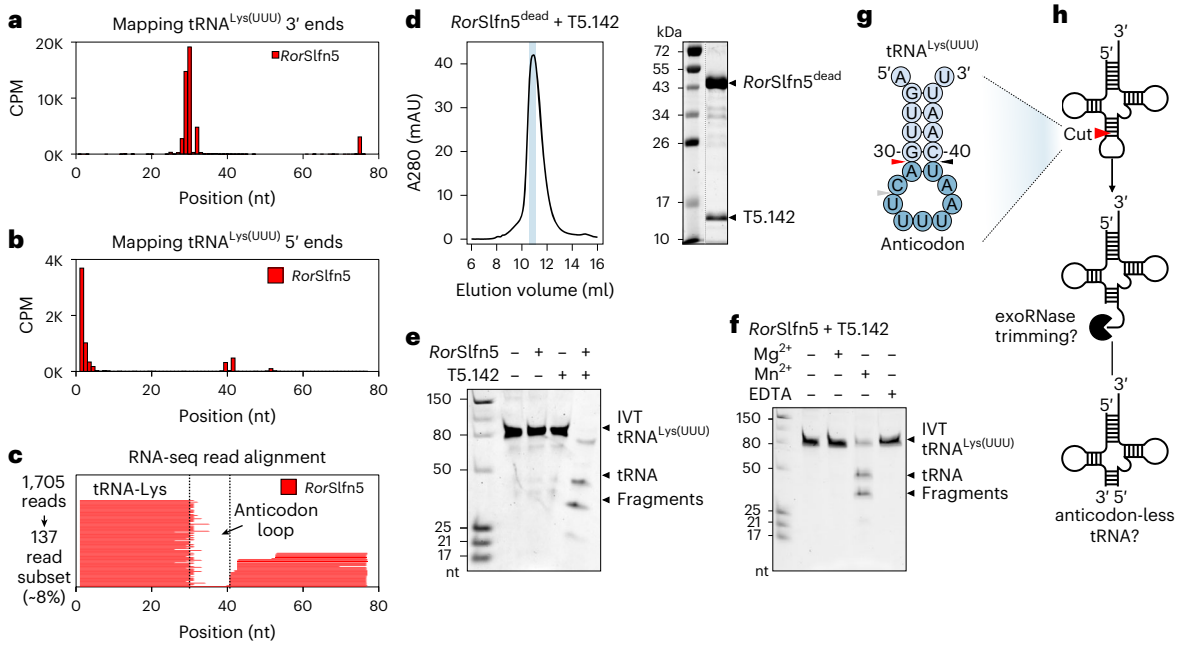

Fig. 5 | Phage-activated *Ror*Slfn5 cleaves the tRNA anticodon arm. **a**,**b**, Position-specific mapping of internal 3′ ends (**a**) and 5′ ends (**b**) in tRNA$^{Lys(UUU)}$ in T5 phage-infected cells expressing *Ror*Slfn5. The data are shown as the mean of three biological replicates. **c**, Alignment of sequencing reads to the lysW gene of MG1655 cells. One representative replicate from three biological replicates is shown. **d**, SEC of affinity-purified complex of *Ror*Slfn5 and T5.142 (left). The elution fraction highlighted with a light blue rectangle was analysed with SDS–PAGE (right). The full SEC profile can be found in Extended Data Fig. 7. **e**, tRNA cleavage assays with 100 nM tRNA$^{Lys(UUU)}$ and 100 nM *Ror*Slfn5 in the presence of T5.142 trigger (2 μM) and Mn^{2+} (2 mM). **f**, The same as in **e** but with 2 mM Mg^{2+}, 2 mM Mn^{2+} or no metal and 10 mM EDTA. All shown assays were reproduced independently three times with similar results. **g**, Potential *Ror*Slfn5 cut sites (triangles) in the anticodon arm of tRNA$^{Lys(UUU)}$, according to RNA-seq data in **a** and **b**. The red triangle shows the cut site supported by cleavage assays in **e** and **f**. **h**, A proposed model for *Ror*Slfn5-mediated tRNA cleavage in vivo and subsequent host exoribonuclease (exoRNase) trimming of the anticodon loop.

RNA from cells at 0, 30 and 60 min post-T5.142 induction. Urea–PAGE analysis of extracted RNA identified RNA fragments between 25 and 50 nt in size that appeared at 30- and 60-min post-induction in cells expressing *Ror*Slfn5 but not the catalytically inactivated mutant, demonstrating that T5.142 expression triggers *Ror*Slfn5-mediated RNA cleavage (Fig. 4g).

To map RNA cleavage induced by *Ror*Slfn5, we performed RNA 3′-end sequencing (Fig. 4h). To validate this approach, we analysed RNA from *E. coli* expressing the PARIS-2 immune system. RNA sequencing (RNA-seq) revealed a significant enrichment of internal 3′ ends in tRNA$^{Lys(UUU)}$ (false discovery rate (FDR) of 0.002) in T5-infected cells expressing the active PARIS-2 defence compared with cells expressing the inactivated PARIS-2 system (AriB^{E26A} mutant; Extended Data Fig. 6a–c). This result agrees with previous work demonstrating that activation of PARIS-2 immunity triggers AriB-mediated cleavage of tRNA$^{Lys(UUU)}$[20,33].

Next, we applied the same RNA-seq strategy to T5 phage-infected MG1655 cells expressing *Ror*Slfn5 or its nuclease-dead mutant (Fig. 4h and Extended Data Fig. 6g). This analysis found no significant difference in the abundance of internal 3′ ends in messenger RNA (mRNA), non-coding RNA (ncRNA) or ribosomal RNA (rRNA), while internal tRNA 3′ ends were significantly enriched in cells expressing WT *Ror*Slfn5 ($P_{adj} = 3.4 \times 10^{-3}$; Fig. 4i). Analysis of tRNA mapping reads identified significant enrichment of total internal 3′-end counts in tRNA$^{Lys(UUU)}$ (194.1-fold, FDR of 2.4×10^{-4}), T5 phage-encoded tRNA$^{Ala(UGC)}$ (34.8-fold, FDR of 5.2×10^{-3}) and tRNA$^{Met(CAU)}$ (145.4-fold, FDR of 4.4×10^{-5}) in cells expressing WT *Ror*Slfn5 compared with the nuclease-dead mutant (Slfn5^{dead}; Fig. 4j and Supplementary Table 7). Position-specific analysis confirmed these enrichments and identified additional tRNAs with significant cleavage signatures, including tRNA$^{Val(UAC)}$, tRNA$^{Phe(GAA)}$ and tRNA$^{Ile(CAU)}$ (FDR <0.05; Extended Data Fig. 6h). Together, these results indicated that *Ror*Slfn5 preferentially cleaves tRNA upon phage infection, with tRNA$^{Lys(UUU)}$ fragments being most abundant in the cell.

Phage-activated *Ror*Slfn5 cleaves the tRNA anticodon arm

We next sought to map *Ror*Slfn5-mediated tRNA cleavage sites at single-nucleotide resolution. Mapping of 3′ ends in tRNA$^{Lys(UUU)}$ identified three highly enriched positions within the anticodon arm (29, 30 and 32), while the 5′-end mapping showed peaks at positions 39 and 41 (Fig. 5a,b). Correspondingly, sequence coverage across the entire anticodon loop of tRNA$^{Lys(UUU)}$ was absent, indicating complete removal of this region (Fig. 5c). A similar sequence coverage gap was observed between the 3′ and 5′ ends of tRNA$^{Met(CAU)}$ fragments (Extended Data Fig. 6i–k,m). This cleavage pattern suggests that *Ror*Slfn5 may either excise the anticodon loop through two precise cuts or perform a single cut followed by trimming of the resulting fragments by host ribonucleases. Supporting the latter model, RNA-seq of cells expressing the PARIS immune system revealed a similar 11-nucleotide gap in the anticodon loop of tRNA$^{Lys(UUU)}$ spanning nucleotides 29 and 41, the latter position matching the AriB cut site identified in vitro[20,33]. These findings support a mechanism in which cleavage is followed by trimming of the anticodon loop (Extended Data Fig. 6d–f,l).

To reconstitute tRNA cleavage in vitro, we expressed and purified *Ror*Slfn5 and T5.142 proteins. The size-exclusion chromatography (SEC) profile of the *Ror*Slfn5 (43.1 kDa) indicates that it assembles in higher-order oligomers, while T5.142 (13.8 kDa) eluted at a size consistent with a dimer or a trimer, based on gel filtration standards (Extended Data Fig. 7a,b). SEC with multi-angle light scattering (SEC–MALS) analysis confirmed this oligomerization, estimating an average mass of 261.0 ± 0.4 kDa, indicating that *Ror*Slfn5 predominantly forms a hexamer at the tested conditions (Extended Data Fig. 7c). As Ig-like domains often mediate protein–protein interactions[34], we hypothesized that the Ig-like domain of *Ror*Slfn5 may detect phage by directly binding T5.142. To test this hypothesis, we co-expressed *Ror*Slfn5^{dead} with the T5.142 and performed a reciprocal affinity co-purification using a Twin-Strep-tag (Extended Data Fig. 7d).

https://doi.org/10.1038/s41564-026-02277-8

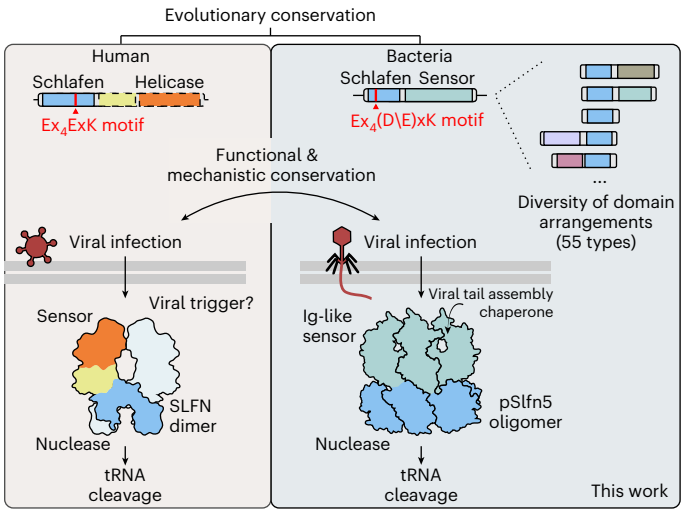

Fig. 6 | Schlafen proteins bridge innate immunity across domains of life. A model for Schlafen-mediated phage defence (right). This mechanism parallels antiviral Schlafen function in humans (left), revealing functional and mechanistic conservation.

Both proteins co-purified from cell lysates regardless of which had the affinity tag and, after cleaving off the tags, *Ror*Slfn5^{dead} and T5.142 co-eluted in a single SEC peak, confirming a direct interaction and suggesting that binding of T5.142 triggers the tRNase activity of *Ror*Slfn5 (Fig. 5d and Extended Data Fig. 7e).

Human SLFN nucleases catalyse tRNA cleavage using a manganese-dependent mechanism[3,4]. To test whether *Ror*Slfn5 shares a similar mechanism, we incubated synthetic tRNA$^{Lys(UUU)}$ with purified *Ror*Slfn5 and T5.142 in the presence of manganese, which yielded two major cleavage fragments sized between 25 and 50 nucleotides (Fig. 5e). Neither protein alone produced detectable cleavage and no activity was observed in the absence of metal or in the presence of EDTA (Fig. 5e,f). The detected tRNase activity was manganese specific as neither magnesium nor any other tested divalent metal supported cleavage in the tested conditions (Fig. 5f and Extended Data Fig. 8a). Mutations in the pSlfn active site (E15A, D20A) abolished cleavage activity, demonstrating that the Slfn nuclease domain of *Ror*Slfn5 catalyses the cleavage reaction (Extended Data Fig. 8b). Upon titration of the trigger, tRNA cleavage was detectable with 1 µM T5.142 (100 nM *Ror*Slfn5, 100 nM tRNA$^{Lys(UUU)}$), while concentrations of T5.142 higher than 2 µM did not further enhance activity, suggesting that this trigger concentration saturates *Ror*Slfn5 under the tested conditions (Extended Data Fig. 8c). Together, these cleavage assays demonstrate that *Ror*Slfn5 functions as a manganese-dependent tRNase, activated by the phage tail assembly chaperone.

Testing additional tRNA substrates showed that bacterial tRNA$^{Lys(UUU)}$ and T5-encoded tRNA$^{Ala(UGC)}$ were cleaved most efficiently, consistent with these tRNAs being the top hits in our RNA-seq data (Fig. 4j and Extended Data Fig. 8d). In vitro cleavage of tRNA$^{Lys(UUU)}$ produced two major products, consistent with a single cut (Fig. 5e,f), while the in vivo RNA-seq data identified two candidate *Ror*Slfn5 cut sites at nucleotides 30–31 (site 1) and 39–40 (site 2) in tRNA$^{Lys(UUU)}$ (Fig. 5g). The fragment sizes observed in vitro support cleavage at predicted site 1 (30- and 46-nt products) over site 2 (37- and 39-nt products) (Fig. 5e,f). We therefore propose that in vivo *Ror*Slfn5 cleaves the anticodon arm between nucleotides 30 and 31 (site 1), which is then followed by trimming of the anticodon loop by host ribonucleases (Fig. 5h).

Discussion

tRNA cleavage as an antiviral strategy was first demonstrated with the discovery of the bacterial PrrC anticodon nuclease[35,36]. Since then, several other examples of anti-phage tRNases have been described, such as AriB from the PARIS system[20], PtuAB from Retron Ec78[37] and ribonucleases in prophage competition elements[38]. More recently, virus-induced tRNA cleavage has also been recognized as a component of antiviral defence in mammals[3,4,12]. Although mechanistically similar, these shared antiviral strategies were thought to have emerged independently through convergent evolution[12]. Our work establishes a direct evolutionary link by demonstrating that homologues of human Schlafen tRNA ribonucleases function in bacterial phage defence through a tRNA cleavage mechanism conserved across the tree of life.

The evolutionary and functional conservation of the Schlafen ribonuclease domain suggests that it belongs to an ancient ancestral immune system that predates the divergence of prokaryotes and eukaryotes[39] (Fig. 6). In prokaryotes, this antiviral effector is fused to a variety of accessory domains that probably act as phage sensors, regulating the nuclease activity in response to distinct viral cues. This modular architecture of Schlafen proteins appears to be a deeply conserved feature, with the core ribonuclease domain fused to diverse regulatory modules in both prokaryotes and mammals[17,40]. Binding of single-stranded DNA (ssDNA) to the helicase domain of human SLFN11 activates its tRNase activity, whereas recent work found that SAMD9, which has a complex multidomain architecture, is activated by cytosolic double-stranded nucleic acids[6,12,41,42]. This recurrent fusion of the Schlafen nuclease with diverse sensory domains highlights its versatility as an antiviral effector, co-opted by immune systems across the domains of life.

Many domains associated with prokaryotic Schlafen have not been previously linked to phage defence, revealing a previously unknown repertoire of phage-sensing mechanisms. In particular, we have identified an uncharacterized C-terminal immunoglobulin-like sensor domain in pSlfn5 that detects tail assembly chaperones of T5-like phages, dictating the phage specificity. We found that phages with substitutions in T5.142 can evade pSlfn5 defence without manifesting any apparent fitness defects. Selection of such escape variants, in turn, might drive adaptations in the sensor domain to regain the defence. Consistent with this co-evolution model, the Slfn nuclease domain is highly conserved across pSlfn5 orthologues, whereas the sensor domain shows greater sequence variation.

Functional, genetic and biochemical assays in our work demonstrate that the T5.142 phage tail assembly chaperone activates *RorSlfn5*, which results in cleavage of the anticodon arm of host- and phage-encoded tRNAs. In this work, we expressed *Ror*Slfn5 under its native promoter in a medium-copy plasmid vector (p15A origin), maintained at ~10–20 copies per cell[43,44], which may result in expression levels higher than physiological. The elevated levels of *Ror*Slfn5 may expand its target RNA specificity beyond that observed under physiological expression. While our data establish trigger-dependent tRNA cleavage by *Ror*Slfn5, additional work would be needed for a more nuanced understanding of its preferred cleavage targets in the native context.

Phage tRNAs often accumulate mutations that make them resistant to cleavage by immune anticodon nucleases[45]. Our work indicates that *Ror*Slfn5 might cleave phage tRNA$^{Ala(UGC)}$ more efficiently than its host equivalent, suggesting that these mutations can backfire, rendering phage tRNAs susceptible. Moreover, phage tRNAs can supplement the cellular tRNA pools, fine-tuning them to the codon usage of late phage genes[46]. Therefore, targeting phage tRNA may be effective for subverting the late stages of infection and limiting phage progeny.

The modular architecture of prokaryotic Schlafen immunity parallels that of recently described single-gene Shedu systems, which pair a shared nuclease core with diverse sensory domains[47–49]. In Shedu, the nuclease forms a central oligomeric core with variable sensors projecting outwards[41,42]. While *Ror*Slfn5 also purifies as a higher-order oligomer, whether oligomerization is driven by the nuclease or the

sensor remains unknown. Structural and biochemical studies will be essential to determine the architecture of this complex, how phage components activate the nuclease, what is the molecular basis for tRNA specificity and whether distinct domain fusions of prokaryotic Schlafens converge on a shared activation mechanism or have evolved unique mechanistic solutions.

Methods

Plasmids, bacterial strains and bacteriophages

The oligonucleotide primers and plasmid DNA sequences are listed in Supplementary Table 4. Candidate phage defence genes with native promoters (100–150 upstream sequence) were synthesized and cloned into a medium-copy plasmid vector (pTwist_Amp_MC) by Twist Bioscience. The plasmid expressing the PARIS-2 immune system of *E. coli* B185 was a gift from Dr. Blake Wiedenheft[20]. Site-directed mutagenesis was used to make nucleotide substitutions in plasmid pAN248 to create the nuclease-dead variant of *Ror*Slfn5 (E15A, D20A mutations) and in plasmid pRF85 to inactivate AriB nuclease (E26A mutation) in the PARIS-2 system. The genes encoding the T5 tail assembly chaperone (T5.142; NCBI accession: YP_006970.1) and its variants (D18G, D68G and I72T) were PCR amplified from genomic DNA of the T5 phage and its escape variants. Amplified genes were cloned into the pBAD vector. Homologues of T5.142 gene were synthesized by Twist Bioscience and cloned into pBAD. To perform the cell toxicity assays, the plasmid backbones of pAN248 (*Ror*Slfn5), pAN254 (*Pag*Slfn5) and pAN294 (*Sfo*Slfn5) were modified to replace the ampicillin resistance (AmpR) gene with the kanamycin resistance (KanR) gene. Plasmids pAN309 and pAN310 expressing chimeras of *Ror*Slfn and *Sfo*Ig-like and *Sfo*Slfn and *Ror*Ig-like were assembled using Hi-Fi (NEB, E2621). Gene fragments for pAN301 (pSOS-GFP) were synthesized by Twist Biosciences and assembled using NEBridge Golden Gate Assembly Kit (BsmBI-v2) (NEB, E1602S). For protein expression, the genes encoding for *Ror*Slfn5 and T5.142 were cloned into the pDF0118 (Addgene #172503) or pRSF-1b vector backbones in frame with a 6xHis-TwinStrep-SUMO affinity tag. All plasmid sequences were confirmed with whole-plasmid sequencing at Plasmidsaurus (https://www.plasmidsaurus.com/). All bacterial strains and phages used in this work are listed in Supplementary Table 4.

Computational search for prokaryotic Slfn

The initial search was done using jackhmmer to find homologues of the human SLFN11 nuclease domain (amino acids 1–354; NCBI: NP_001098057.1) in a database of reference proteomes[50]. The hidden Markov model (HMM) generated by jackhmmer was used to perform an HMMsearch (from HMMER 3.1b2) on a database of bacterial and archaeal amino acid sequences, created by translating RefSeq complete genomes, downloaded in July 2023, using prodigal[51]. The non-redundant hits from the first HMMsearch (e-value <0.001; CD-HIT with -c 0.9) were aligned using MAFFT v7.526. A new HMM was created from the alignment using HMMbuild and HMMsearch was repeated on the same database. The second round found 9,937 potential homologues (e-value <0.001) with full-length Slfn domains (>100 amino acids; PF04326). After redundancy (CD-HIT with -c 1) was removed, a total of 5,930 protein sequences were left.

Prokaryotic Slfn domains were mapped in the HMMsearch hits using HMMscan with the PF04326.19 HMM profile from the Pfam database[25]. Prokaryotic Slfn domains (5,930) were extracted and aligned using MAFFT v7.526 with 596 unique mammalian Slfn domain sequences (CD-HIT with -c 1) found with jackhmmer. The resulting alignment was used to build a phylogenetic tree using FastTree v2.1.11 with -pseudo -wag -gamma options. For visualization, the tree was pruned to remove prokaryotic sequences with >50% sequence similarity (CD-HIT -c 0.5) and mammalian sequences with >70% sequence similarity (CD-HIT -c 0.7). The resulting tree was visualized and annotated using iTOL[52].

For every identified pSlfn, genes within a ±10-kbp distance were extracted and annotated using HMMscan (i-E-value <0.001) against HMM profiles downloaded from the DefenseFinder database in March 2025[53]. The number of defence genes identified in the genetic proximity was then calculated for every pSlfn gene (Supplementary Table 1). Defence scores were calculated for pSlfn clusters as the number of pSlfn homologues with at least one annotated defence gene in the genetic neighbourhood divided by the total number of pSlfn homologues within the cluster.

Classification of pSlfn proteins

Sequences of 5,930 pSlfn proteins were searched against the Pfam database[25] (v37.2) using HMMER's hmmscan[50], and against the ECOD database[26] (v292) using BLAST[54]. Pfam hits (i-E-value <0.0001) were filtered to remove overlapping or nested annotations by selecting predictions with the highest confidence. Proteins with significant sequence homology to multiple Pfam families, that is, fusions of Slfn (PF04326) to other domains, were further classified by assignment to their respective Pfam clan, representing a higher-order grouping of related domain families. Proteins with Slfn domains and less than 40 amino acids of remaining sequence were annotated as 'pSlfn only'. Proteins with Slfn domains and more than 40 amino acids of remaining sequence without confident hits to Pfam or ECOD (2,134 total) were further annotated using structural homology as described before[55]. Briefly, 2,134 proteins were grouped in 903 clusters using MMseqs with 50% sequence identity and 0.8 coverage cut offs[56]. AlphaFold 3 (AF3) was used to predict protein structure models for each cluster representative[57]. AF3 models were processed by Domain Parser for AlphaFold Models (DPAM) to identify domain architectures and map domains to the ECOD database classification[58]. The resulting ECOD domain classifications were assigned to cluster members, converted into corresponding Pfam clans (where possible) and integrated with the sequence-based Pfam domain annotation. For 1,020 pSlfn proteins, a confident annotation could not be assigned. These proteins were designated as unannotated fusions of pSlfn domains and grouped into 558 sequence similarity groups using MMseqs. The domain annotations can be found in Supplementary Table 2.

Computational search for T5.142 homologues

Homologues of T5.142 were identified in the database of non-redundant protein sequences (NCBI) using PSI-BLAST. Identified homologues were clustered using CD-HIT with -c 0.9, and cluster representatives were used for experimental testing. Protein sequences of T5.142 homologues were aligned with MAFFT v7.526. The phylogenetic tree was constructed using FastTree v2.1.11 with -pseudo -wag -gamma options and visualized using iTOL.

Bacterial growth assays

E. coli K-12 MG1655 cells expressing *Ror*Slfn5, *Ror*Slfn5$^{E15A, D20A}$ or carrying no defence system were grown with shaking at 37 °C to an OD_{600} of 0.3. Then, 180 µl of the cell culture was transferred to a 96-well plate and mixed with 20 µl of T5 phage dilution at varying MOIs. The 96-wells were shaken and the OD_{600} was measured every 60 s for 6 h at 37 °C using a SpectraMax M5e reader. To measure bacterial growth upon viral trigger expression, *E. coli* K-12 MG1655 cells were co-transformed with *Ror*Slfn5 or *Ror*Slfn5^{E15A,D20A} and a plasmid with an inducible trigger T5.142 or GFP gene. Double-transformed cells were plated on LB agar plates with dual antibiotics and 0.2% glucose to suppress basal expression. Night cultures of double-transformed cells were used to inoculate liquid cultures and cells were grown to an OD_{600} of 0.3. After reaching optical density, 180 µl of bacterial cultures were mixed with 20 µl of D-glucose or L-arabinose to a final concentration of 0.2% in a 96-well plate. Optical density and GFP signal were measured every 60 s for 6 h at 37 °C using a SpectraMax M5e reader. All experiments were performed in three or four biological replicates.

EOP assay

E. coli K-12 MG1655 or *E. coli* NovaBlue (for testing phages M13, MS2 and Qbeta) expressing candidate phage defence genes, the PARIS-2 system or an EV (negative control) were grown in LB medium with shaking at 37 °C to an OD_{600} of 0.3. Cultures were supplemented with antibiotics, 10 mM $MgCl_2$ and 10 mM $CaCl_2$. Day cultures were then mixed with soft agar containing the same supplements and antibiotics and overlaid onto LB agar plates. The plates were allowed to dry for 1 h at room temperature. Serial dilutions of phages were prepared and 10 µl of each dilution was spotted onto the plates and left to dry until the drops were no longer visible. Plates were incubated overnight at 37 °C. The following day, the phage titre (PFU ml^{-1}) was determined from the dilution that produced countable plaques. For T2, T4 with PARIS-2, M13, MS2 and Qbeta phages, the least concentrated dilution that yielded full lysis was considered to be 100 plaques following previously published methods[59]. The EOP was calculated as the ratio of the phage titre with cells expressing the immune system to that of the EV control. All experiments were performed in three biological replicates.

ECOI assays

Day cultures of *E. coli* K-12 MG1655 cells expressing either an EV or *Ror*Slfn5 defence system were grown as previously described. Once OD_{600} reached 0.3, 1 ml of cells was infected with T5 bacteriophage at 0.1 MOI and incubated at 37 °C for 10 min to allow phage adsorption. Immediately after, samples were centrifuged at 4 °C, 3,000*g* for 5 min, washed twice with SM buffer (50 mM Tris–HCl, pH 7.5, 100 mM NaCl, 8 mM $MgSO_4$ and 0.01% gelatin) and serially diluted. Ten microlitres of diluted cells was spotted onto plates containing bottom agar and soft agar mixed with naive *E. coli* K-12 MG1655 cells (OD_{600} of 0.3) supplemented with 10 mM $MgCl_2$ and 10 mM $CaCl_2$. Plates were dried at room temperature and incubated at 37 °C overnight. The next day, the infection centres were counted and the ECOI was calculated as the ratio of the phage titre on cells expressing the *Ror*Slfn5 candidate defences to that on cells expressing the EV control. All experiments were performed in three biological replicates.

Burst size

Average burst sizes were quantified as previously described with modifications[60]. *E. coli* K-12 MG1655 cells expressing either an EV or *Ror*Slfn5 defence system were grown to an OD_{600} of 0.3. Cells (2 ml) were infected with T5 phage at an MOI of 0.1 and incubated with shaking (180 rpm) for 0, 20 or 60 min. At each time point, 200 µl of cells were mixed with 800 µl of SM buffer with chloroform (2% final). Samples were serially diluted and 10 µl was spotted onto plates containing bottom agar and soft agar mixed with naive *E. coli* K-12 MG1655 cells (OD_{600} of 0.3) and supplements (10 mM $MgCl_2$ and 10 mM $CaCl_2$). Plates were dried at room temperature and incubated overnight at 37 °C. Phage titres (PFU ml^{-1}) were determined the following day and burst size was calculated using the following formula: burst size = (PFU ml^{-1} at 60 min) − (PFU ml^{-1} at 20 min)/(PFU ml^{-1} at 0 min) − (PFU ml^{-1} at 20 min). The experiment was performed in three biological replicates.

Phage escapers isolation

The T5 phage was serially diluted and 100 µl of each dilution was mixed with 500 µl of *E. coli* K-12 MG1655 cells expressing *Ror*Slfn5 at an OD_{600} of 0.3. This mixture was added to 8 ml of soft agar supplemented with ampicillin (100 µg ml^{-1}), 10 mM $MgCl_2$ and 10 mM $CaCl_2$ and overlaid onto LB agar plates containing the same supplements. Plates were incubated overnight at 37 °C. The following day, several individual plaques were picked to inoculate *E. coli* K-12 MG1655 expressing *Ror*Slfn5 (OD_{600} of 0.3). The cultures were incubated overnight in LB media supplemented with ampicillin (100 µg ml^{-1}) at 37 °C with shaking at 180 rpm. The next day, cultures were centrifuged at 5,000*g* for 10 min at 4 °C and the supernatants containing phages were transferred to fresh tubes. The phages were serially diluted and spotted on the lawns of *E. coli* K-12 MG1655 cells expressing *Ror*Slfn5 or no system to assess their ability to escape the immune system.

Phage genomic DNA isolation and sequencing

Genomic DNA of T5 phage and T5 phage escapers was isolated from 1 ml of phage supernatant using Norgen Biotek Phage DNA Isolation Spin Column kit (SKU 46800). Then 500 ng of each genomic DNA sample was used to prepare a sequencing library as described in the SQK-LSK114 protocol using the Native Barcoding kit 24 V14 (SQK-NBD114.24). The flow cell was primed and the barcoded sequencing library (300 ng) was loaded according to the Oxford Nanopore protocol (SQK-LSK114). Raw sequencing data (POD5 files) were base called in the super-accuracy mode (dna_r10.4.1_e8.2_400bps_sup@v5.0.0) and demultiplexed using Dorado basecaller v0.8.3 (Oxford Nanopore). Base-called reads were aligned to the reference (NCBI: NC_005859.1) using minimap2 (v2.28-r1209) with Nanopore preset (-ax map-ont setting). Resulting alignments (BAM files) were used to call consensus sequences using samtools v1.21 and call sequence variants using bcftools v1.21.

Cell toxicity assay

E. coli K-12 MG1655 cells were co-transformed with plasmids encoding for defence systems and inducible pBAD vectors with viral trigger genes or GFP. Double-transformed cells were selected by plating on LB agar supplemented with ampicillin (100 µg ml^{-1}), kanamycin (100 µg ml^{-1}) and D-glucose (0.2%), followed by overnight incubation at 37 °C. Individual colonies were then used to inoculate overnight cultures in LB medium containing the same antibiotics. The following day, cultures were adjusted to OD_{600} of 0.6, tenfold serially diluted and 3 µl of each dilution was spotted onto LB agar plates supplemented with ampicillin (100 µg ml^{-1}), kanamycin (100 µg ml^{-1}) and either 0.2% D-glucose or 0.2% L-arabinose. The resulting plates were incubated overnight at 37 °C. All experiments were performed in three biological replicates.

SOS response reporter assay

E. coli K-12 MG1655 cells were co-transformed with *Ror*Slfn5 or *Ror*Slfn5$^{E15A, D20A}$ plasmid, pBAD plasmid with T5.142 or GFP gene and pSOS-GFP reporter plasmid. Triple-transformed cells were grown to an OD_{600} of 0.3 and 180 µl of these cultures were mixed with 20 µl of D-glucose or L-arabinose to a final concentration of 0.2% in a 96-well plate. Bacterial growth (OD_{600}) and GFP signal were measured every 60 s for 6 h at 37 °C using a SpectraMax M5e reader. Mitomycin C (RPI #M92010) was added to the bacterial culture to a final concentration of 100 nM as a positive control to induce the SOS response. PBS was used as a negative control. All experiments were performed in three biological replicates.

Total RNA extraction

E. coli K-12 MG1655 cells were double transformed with plasmids expressing either *Ror*Slfn5 or *Ror*Slfn5$^{E15A, D20A}$, along with a plasmid encoding the viral trigger T5.142. Cultures were grown to an OD_{600} of 0.3 and trigger expression was induced by adding L-arabinose to 0.2% final concentration. Cells were collected at 0, 30 and 60 min post-induction for total RNA extraction using the Direct-zol RNA Miniprep kit (Zymo Research, R2052). Briefly, the cells were spun down at 3,000*g* for 5 min at 4 °C. The supernatants were removed and the cell pellets were resuspended in 900 µl of TRI-reagent (Sigma-Aldrich). Then, the samples in TRI-reagent were loaded on columns and total RNA purification was performed according to the kit instructions with a DNAse I on-column treatment step. Then ~500 ng of total RNA was used to run a 12% urea–PAGE. The *E. coli* K-12 MG1655 cell cultures expressing *Ror*Slfn5, *Ror*Slfn5$^{E15A, D20A}$, PARIS or PARIS$^{AriB(E26A)}$ (OD_{600} of 0.3) were infected with T5 phage at an MOI of 10. Culture samples (5 ml) were taken right before the infection (0 min) and 30 min after for total RNA extraction using the Direct-zol RNA Miniprep kit from Zymo Research (R2052) as described above. The quality of RNA samples was assessed

using the Agilent 2100 Bioanalyzer at the University of Florida ICBR Gene Expression and Genotyping Core Facility (RRID: SCR_019145).

RNA-seq

Total RNA samples (~1,200 ng each) were treated with T4 PNK (NEB, M0201) in a reaction buffer (50 mM Tris–HCL, pH 7.5, 10 mM $MgCl_2$, 1 mM DTT, 1 mM ATP and murine RNase inhibitor 1 U μl^{-1} (NEB)) for 1 h at 37 °C. Next, RNA was purified with the Monarch RNA Cleanup kit (NEB, T2030L). PNK-treated RNA samples were polyadenylated using *E. coli* Poly(A) polymerase (NEB, M0276S) in a reaction buffer (50 mM Tris–HCl, pH 8.0, 250 mM NaCl, 10 mM $MgCl_2$, 1 mM ATP and murine RNase inhibitor 1 U μl^{-1}) for 30 min at 37 °C. The RNA samples were purified with the Monarch RNA Cleanup kit (NEB, T2030L) and sonicated with a Bioruptor Pico sonication device. For shearing, RNA samples were diluted in TE buffer (10 mM Tris–HCl, pH 8.0, and 1 mM EDTA) to 50 µl and sonicated for 30 cycles, with 30 s of ON time and 30 s of OFF time (15 min total sonication time). RNA was purified with RNA-Clean XP beads (Beckman Coulter, A63987) using a 2:1 ratio of beads to RNA (v/v) and used to prepare a sequencing library as described in the SQK-PCB114.24 protocol using Barcoding kit CDNA-PCR 24 V14 (Oxford Nanopore). Briefly, the RNA was reverse transcribed and the resulting cDNA was amplified with barcoded PCR primers. Barcoded PCR products were purified using Mag-Bind TotalPure NGS magnetic beads (Omega Bio-tek) and pooled together for sequencing library preparation. The flow cell was primed and the barcoded sequencing library (~10 ng) was loaded according to the Oxford Nanopore protocol (SQK-PCB114.24). Raw sequencing data (POD5 files) were base called using the super-accuracy model (dna_r10.4.1_e8.2_400bps_sup@v5.0.0) and demultiplexed with Dorado basecaller, v0.9.1, with the --no-trim option (Oxford Nanopore). Primer sequences and polyA (sense strand reads) or polyT (anti-sense strand reads) tails were removed using cutadapt v5.0. Bowtie 2 (v2.5.4) was used to align trimmed reads to a reference sequence created by concatenating sequences of the *E. coli* K-12 MG1655 genome (NCBI: NC_000913.3), the T5 phage genome (NCBI: NC_005859.1) and the pAN248 plasmid (this work). To map RNA ends, start and end coordinates for every read were extracted using bedtools bamtobed (v2.31.1). RNA end coordinates were mapped to genetic features, quantified and normalized using total mapped read counts to produce count per million mapped reads (CPM) values. RNA ends were classified as internal if the RNA end position was >10 nucleotides from the transcript start and transcript end. Read alignments were plotted using Gviz v1.44.2 R package.

Protein expression and purification

For individual protein expression and purification, the vectors pAN261 (6xHisTwinStrepSUMO-*Ror*Slfn5) and pAN302 (6xHisTwinStrepSUMO-T5.142) were transformed into T7 Express lysY cells (NEB, C3010I). Cells were grown in LB broth (Lennox) supplemented with ampicillin (100 µg ml^{-1}) at 37 °C to an OD_{600} of 0.5–0.7, incubated on ice for 30 min and then induced with 0.5 mM IPTG for overnight expression at 16 °C. Cells were lysed with sonication in lysis buffer (20 mM Tris–HCl pH 8.0, 500 mM NaCl, 1 mM TCEP and protease inhibitor (PI78430, Thermo Fisher)). Lysates were clarified by sequential centrifugation: first at 10,000*g* for 20 min at 4 °C and then the supernatant was re-centrifuged at 10,000*g* for an additional 10 min at 4 °C. The affinity-tagged proteins were bound to StrepTrap XT-columns (Cytiva) and eluted with elution buffer (20 mM Tris–HCl pH 8.0, 500 mM NaCl, 1 mM TCEP and 50 mM Biotin). Proteins were concentrated using 10-kDa spin concentrators. Affinity tags were removed by overnight dialysis at 4 °C against SUMO digest buffer (30 mM Tris–HCl pH 8.0, 500 mM NaCl, 1 mM TCEP and 0.15% Igepal) with His-tagged SUMO protease made in house. The affinity tag and protease were removed using a HisTrap HP column (Cytiva) and the flow-through containing untagged *Ror*Slfn5 or T5.142 was concentrated using Corning Spin-X concentrators at 4 °C. Finally, the proteins were purified using a Superdex 200 10/300 size-exclusion column (Cytiva) in a buffer (20 mM Tris–HCl, pH 7.5, 500 mM NaCl and 1 mM TCEP). Fractions containing the target protein were pooled, concentrated, aliquoted, flash-frozen in liquid nitrogen and stored at −80 °C.

For SEC–MALS analysis of *Ror*Slfn5, the protein was first purified as described above; then 100 µl of pooled SEC peak fractions was loaded again on the Superdex 200 10/300 column equilibrated with SEC buffer and passed through a miniDAWN MALS detector and an Optilab refractive index detector (Wyatt Technology). Data collection and analysis were performed using the ASTRA v8.1.2.1 software (Wyatt Technology).

For the purification of the *Ror*Slfn5-T5.142 complex, two co-expression schemes were used. 6xHisTwinStrepSUMO-tagged *Ror*Slfn5^{E15A,D20A} (pAN372) was co-expressed with untagged T5.142 (pAN316), or untagged *Ror*Slfn5 (pAN338) was co-expressed with 6xHisTwinStrepSUMO-tagged T5.142 (pAN302) in T7 Express *lysY E. coli*. The cells were grown to an OD_{600} of 0.5 and induced with 0.5 mM IPTG at 16 °C. Cell pellets were lysed with sonication in Lysis buffer (20 mM Tris–HCl, pH 8.0, 500 mM NaCl, 1 mM TCEP and protease inhibitor (PI78430, Thermo Fisher)) and lysates were clarified by centrifugation as described above. The Strep-tagged complex was affinity purified from the lysates using a StrepTrap XT column. For SEC, the affinity tag was removed and the complex was loaded on the Superdex 200 10/300 gel filtration column (Cytiva), as described above.

tRNA synthesis

Bacterial and T5 phage tRNA were synthesized using in vitro transcription (IVT) as previously described[33]. Briefly, single-stranded DNA oligos encoding tRNA with an upstream T7 promoter sequence were ordered from Eurofins Genomics (Supplementary Table 4) and used as templates for PCR. Each 25 µl PCR reaction contained 1× Q5 Reaction Buffer (NEB), 200 µM dNTPs, 0.5 µM forward primer, 0.5 µM reverse primer, 0.2 U μl^{-1} Q5 High-Fidelity DNA Polymerase (NEB) and 0.04 µM of DNA oligo template. PCR products were purified using the DNA Clean and Concentrator-5 kit (Zymo Research, D4014). To synthesize tRNA, 0.8–1 µg of PCR product was used as a template for an IVT reaction using the HiScribe T7 High Yield RNA Synthesis kit (NEB, E2040L). The 10 µl reactions were prepared following the manufacturer's instructions and incubated for 16–18 h at 37 °C. IVT products were treated with DNase I (NEB, M0303L) and then purified using the Monarch RNA Cleanup kit (NEB, T2050S).

tRNA cleavage assay

To test RorSlfn5 nuclease activity in vitro, 100 nM of *Ror*Slfn5 or *Ror*Slfn5$^{E15A, D20A}$ was incubated with 100 nM of tRNA with or without the purified T5.142 trigger in the reaction buffer (50 mM Tris–HCl, pH 7.5, 2 mM $MnCl_2$, 100 mM NaCl and 1 mM DTT). To test other divalent metals, $MgCl_2$, $CaCl_2$, $ZnCl_2$ or $NiSO_4$ were used instead of $MnCl_2$ in the same buffer conditions. All reactions were incubated for 1 h at 37 °C, and 50 mM EDTA was added to stop the reaction. Samples were incubated for 10 min at 70 °C with 2× RNA loading dye before loading into a preheated 15% urea–PAGE. The gel was run at 20 W, stained with SYBR Gold (Invitrogen, S11494) for 30 min and imaged on a Bio-Rad Chemidoc MP Imaging System.

Statistics and reproducibility

Statistical analyses were performed using R version 4.3.0 with functions from the stats package. Experiments that compare three or more groups were analysed using a one-way analysis of variance (ANOVA). Post-hoc pairwise mean comparisons were performed using Tukey's honestly significant difference (HSD) or Dunnett's test. Means in experiments with two groups were compared using a two-sided Welch's *t*-test. For RNA-seq data, normalized (CPM) and $\log_2$-transformed RNA end counts were compared using a two-sided Welch's *t*-test with unequal variances and the resulting *P* values were adjusted using the Holm method or Benjamini–Hochberg correction to calculate the FDR.

The statistical test, the level of statistical significance and the sample size (n) for each experiment are provided in the figure legends. Results of all statistical tests and exact P values are provided in the Source Data. Data were plotted using the ggplot2 and pheatmap packages in R.

Reporting summary

Further information on research design is available in the Nature Portfolio Reporting Summary linked to this article.

Data availability

Raw sequencing data were deposited in the NCBI Sequence Read Archive and are publicly available under Bioproject accession numbers PRJNA1272589 (phage genome sequencing) and PRJNA1272590 (3′-end RNA sequencing). Source data are provided with this paper.

References

1. Schwarz, D. A., Katayama, C. D. & Hedrick, S. M. Schlafen, a new family of growth regulatory genes that affect thymocyte development. *Immunity* **9**, 657–668 (1998).
2. Li, M. et al. DNA damage-induced cell death relies on SLFN11-dependent cleavage of distinct type II tRNAs. *Nat. Struct. Mol. Biol.* **25**, 1047–1058 (2018).
3. Yang, J.-Y. et al. Structure of Schlafen13 reveals a new class of tRNA/rRNA-targeting RNase engaged in translational control. *Nat. Commun.* **9**, 1165 (2018).
4. Metzner, F. J. et al. Mechanistic understanding of human SLFN11. *Nat. Commun.* **13**, 5464 (2022).
5. Li, M. et al. Codon-usage-based inhibition of HIV protein synthesis by human schlafen 11. *Nature* **491**, 125–128 (2012).
6. Zhang, P. et al. Schlafen 11 triggers innate immune responses through its ribonuclease activity upon detection of single-stranded DNA. *Sci. Immunol.* **9**, eadj5465 (2024).
7. Jo, U. & Pommier, Y. Structural, molecular, and functional insights into Schlafen proteins. *Exp. Mol. Med.* **54**, 730–738 (2022).
8. Kim, E. T. & Weitzman, M. D. Schlafens can put viruses to sleep. *Viruses* **14**, 442 (2022).
9. Nightingale, K. et al. Human cytomegalovirus protein RL1 degrades the antiviral factor SLFN11 via recruitment of the CRL4 E3 ubiquitin ligase complex. *Proc. Natl Acad. Sci. USA* **119**, e2108173119 (2022).
10. Valdez, F. et al. Schlafen 11 restricts flavivirus replication. *J. Virol.* **93**, e00104–e00119 (2019).
11. Xie, X. et al. SAMD9L acts as an antiviral factor against HIV-1 and primate lentiviruses by restricting viral and cellular translation. *PLoS Biol.* **22**, e3002696 (2024).
12. Zhang, F. et al. Human SAMD9 is a poxvirus-activatable anticodon nuclease inhibiting codon-specific protein synthesis. *Sci. Adv.* **9**, eadh8502 (2023).
13. Podvalnaya, N. et al. piRNA processing by a trimeric Schlafen-domain nuclease. *Nature* **622**, 402–409 (2023).
14. Bustos, O. et al. Evolution of the Schlafen genes, a gene family associated with embryonic lethality, meiotic drive, immune processes and orthopoxvirus virulence. *Gene* **447**, 1–11 (2009).
15. Makarova, K. S., Wolf, Y. I., Snir, S. & Koonin, E. V. Defense islands in bacterial and archaeal genomes and prediction of novel defense systems. *J. Bacteriol.* **193**, 6039–6056 (2011).
16. Aravind, L., Nicastro, G. G., Iyer, L. M. & Burroughs, A. M. The prokaryotic roots of eukaryotic immune systems. *Annu. Rev. Genet.* **58**, 365–389 (2024).
17. Burroughs, A. M., Aravind, L. & Stock, A. M. Identification of uncharacterized components of prokaryotic immune systems and their diverse eukaryotic reformulations. *J. Bacteriol.* **202**, e00365–20 (2020).
18. Kibby, E. M. et al. Bacterial NLR-related proteins protect against phage. *Cell* **186**, 2410–2424 (2023).
19. Makarova, K. S., Wolf, Y. I. & Koonin, E. V. Comparative genomics of defense systems in archaea and bacteria. *Nucleic Acids Res.* **41**, 4360–4377 (2013).
20. Burman, N. et al. A virally encoded tRNA neutralizes the PARIS antiviral defence system. *Nature* **634**, 424–431 (2024).
21. Rousset, F. et al. Phages and their satellites encode hotspots of antiviral systems. *Cell Host Microbe* **30**, 740–753 (2022).
22. Fillol-Salom, A. et al. Bacteriophages benefit from mobilizing pathogenicity islands encoding immune systems against competitors. *Cell* **185**, 3248–3262 (2022).
23. Georjon, H. & Bernheim, A. The highly diverse antiphage defence systems of bacteria. *Nat. Rev. Microbiol.* **21**, 686–700 (2023).
24. Rousset, F. & Sorek, R. The evolutionary success of regulated cell death in bacterial immunity. *Curr. Opin. Microbiol.* **74**, 102312 (2023).
25. Paysan-Lafosse, T. et al. The Pfam protein families database: embracing AI/ML. *Nucleic Acids Res.* **53**, D523–D534 (2025).
26. Schaeffer, R. D. et al. ECOD: integrating classifications of protein domains from experimental and predicted structures. *Nucleic Acids Res.* **53**, D411–D418 (2025).
27. Zweig, M., Rosenkranz, H. S. & Morgan, C. Development of coliphage T5: ultrastructural and biochemical studies. *J. Virol.* **9**, 526–543 (1972).
28. Lopatina, A., Tal, N. & Sorek, R. Abortive infection: bacterial suicide as an antiviral immune strategy. *Annu. Rev. Virol.* **7**, 371–384 (2020).
29. Aframian, N. & Eldar, A. Abortive infection antiphage defense systems: separating mechanism and phenotype. *Trends Microbiol.* **31**, 1003–1012 (2023).
30. Moineau, S., Durmaz, E., Pandian, S. & Klaenhammer, T. R. Differentiation of two abortive mechanisms by using monoclonal antibodies directed toward lactococcal bacteriophage capsid proteins. *Appl. Environ. Microbiol.* **59**, 208–212 (1993).
31. Hyman, P. & Abedon, S. T. Bacteriophage host range and bacterial resistance. *Adv. Appl. Microbiol.* **70**, 217–248 (2010).
32. Zivanovic, Y. et al. Insights into bacteriophage T5 structure from analysis of its morphogenesis genes and protein components. *J. Virol.* **88**, 1162–1174 (2014).
33. Belukhina, S. et al. Specificity and mechanism of tRNA cleavage by the AriB Toprim nuclease of the PARIS bacterial immune system. *Philos. Trans. R Soc. Lond. B Biol. Sci.* **380**, 20240074 (2025).
34. Chatterjee, S., Basak, A. J., Nair, A. V., Duraivelan, K. & Samanta, D. Immunoglobulin-fold containing bacterial adhesins: molecular and structural perspectives in host tissue colonization and infection. *FEMS Microbiol. Lett.* **368**, fnaa220 (2021).
35. David, M., Borasio, G. D. & Kaufmann, G. Bacteriophage T4-induced anticodon-loop nuclease detected in a host strain restrictive to RNA ligase mutants. *Proc. Natl Acad. Sci. USA* **79**, 7097–7101 (1982).
36. Levitz, R. et al. The optional *E. coli* prr locus encodes a latent form of phage T4-induced anticodon nuclease. *EMBO J.* **9**, 1383–1389 (1990).
37. Azam, A. H. et al. Evasion of antiviral bacterial immunity by phage tRNAs. *Nat. Commun.* **15**, 9586 (2024).
38. Sargen, M. R. & Helaine, S. A prophage competition element protects Salmonella from lysis. *Cell Host Microbe* **32**, 2063–2079 (2024).
39. Bernheim, A., Cury, J. & Poirier, E. Z. The immune modules conserved across the tree of life: towards a definition of ancestral immunity. *PLoS Biol.* **22**, e3002717 (2024).
40. Mekhedov, S. L., Makarova, K. S. & Koonin, E. V. The complex domain architecture of SAMD9 family proteins, predicted STAND-like NTPases, suggests new links to inflammation and apoptosis. *Biol. Direct* **12**, 13 (2017).

41. Peng, S. et al. Structure and function of an effector domain in antiviral factors and tumor suppressors SAMD9 and SAMD9L. *Proc. Natl Acad. Sci. USA* **119**, e2116550119 (2022).
42. Hou, G. et al. SAMD9 senses cytosolic double-stranded nucleic acids in epithelial and mesenchymal cells to induce antiviral immunity. *Nat. Commun.* **16**, 3756 (2025).
43. Jahn, M., Vorpahl, C., Hübschmann, T., Harms, H. & Müller, S. Copy number variability of expression plasmids determined by cell sorting and droplet digital PCR. *Microb. Cell Fact.* **15**, 211 (2016).
44. Shao, B. et al. Single-cell measurement of plasmid copy number and promoter activity. *Nat. Commun.* **12**, 1475 (2021).
45. van den Berg, D. F., van der Steen, B. A., Costa, A. R. & Brouns, S. J. J. Phage tRNAs evade tRNA-targeting host defenses through anticodon loop mutations. *eLife* **12**, e85183 (2023).
46. van den Berg, D. F. & Brouns, S. J. J. Phage tRNAs: decoding the enigma. *Trends Microbiol.* **33**, 1121–1131 (2025).
47. Doron, S. et al. Systematic discovery of antiphage defense systems in the microbial pangenome. *Science* **359**, eaar4120 (2018).
48. Gu, Y. et al. Bacterial Shedu immune nucleases share a common enzymatic core regulated by diverse sensor domains. *Mol. Cell* **85**, 523–536.e6 (2025).
49. Loeff, L., Walter, A., Rosalen, G. T. & Jinek, M. DNA end sensing and cleavage by the Shedu anti-phage defense system. *Cell* **188**, 721–733 (2025).
50. Potter, S. C. et al. HMMER web server: 2018 update. *Nucleic Acids Res.* **46**, W200–W204 (2018).
51. Hyatt, D. et al. Prodigal: prokaryotic gene recognition and translation initiation site identification. *BMC Bioinformatics* **11**, 119 (2010).
52. Letunic, I. & Bork, P. Interactive Tree of Life (iTOL) v6: recent updates to the phylogenetic tree display and annotation tool. *Nucleic Acids Res.* **52**, W78–W82 (2024).
53. Tesson, F. et al. Systematic and quantitative view of the antiviral arsenal of prokaryotes. *Nat. Commun.* **13**, 2561 (2022).
54. Altschul, S. F., Gish, W., Miller, W., Myers, E. W. & Lipman, D. J. Basic local alignment search tool. *J. Mol. Biol.* **215**, 403–410 (1990).
55. Medvedev, K. E. et al. Structure classification of the proteins from *Salmonella enterica* pangenome revealed novel potential pathogenicity islands. *Sci. Rep.* **14**, 12260 (2024).
56. Steinegger, M. & Soding, J. MMseqs2 enables sensitive protein sequence searching for the analysis of massive data sets. *Nat. Biotechnol.* **35**, 1026–1028 (2017).
57. Abramson, J. et al. Accurate structure prediction of biomolecular interactions with AlphaFold 3. *Nature* **630**, 493–500 (2024).
58. Zhang, J., Schaeffer, R. D., Durham, J., Cong, Q. & Grishin, N. V. DPAM: a domain parser for AlphaFold models. *Protein Sci.* **32**, e4548 (2023).
59. Ofir, G. et al. Antiviral activity of bacterial TIR domains via immune signalling molecules. *Nature* **600**, 116–120 (2021).
60. Watson, B. N. J. et al. Type I-F CRISPR–Cas resistance against virulent phages results in abortive infection and provides population-level immunity. *Nat. Commun.* **10**, 5526 (2019).

Acknowledgements

We thank B. Wiedenheft and R. Wilkinson for generous discussions and for sharing *E. coli* strains and bacteriophages; M. Jinek for insightful discussions and valuable advice throughout the course of this work; M. Kladde and M. Gauthier for Bioruptor Pico sonicator access; M. Buyukyoruk for advice on computational analyses; and University of Florida ICBR Gene Expression and Genotyping Core Facility for RNA analysis using the Agilent 2100 Bioanalyzer (RRID: SCR_019145). A. Nemudryi was supported by a start-up package from the University of Florida College of Medicine, University of Florida Office of the Vice President for Research, and University of Florida Emerging Pathogens Institute. This work was supported by the National Institutes of Health grant R00AI171893 (A. Nemudryi) and 1T32GM156737-01 (V.P.T.). L.L. was supported by the LUMC Junior Principal Investigator grant 2025.

Author contributions

A. Nemudryi and A. Nemudraia conceived, designed and supervised the project. A. Nemudryi performed the initial bioinformatic search and neighbourhood analysis. K.E.M. performed classification of pSlfn domain architectures. A. Nemudryi, A. Nemudraia, R.C. and V.P.T. designed and generated the plasmids. A. Nemudraia, V.P.T. and R.C. performed phage assays. A. Nemudryi performed a bacterial growth assay. A. Nemudraia and A. Nemudryi performed phage escaper isolation and sequencing. A. Nemudryi and V.P.T. performed the cell toxicity assays. A. Nemudryi and A. Nemudraia performed RNA extractions and sequencing experiments. A. Nemudryi, A. Nemudraia, Y.W. and L.L. performed protein expression and purification. V.P.T. performed tRNA synthesis and tRNA cleavage assays. A. Nemudryi and A. Nemudraia wrote the original draft, with input from all authors.

Competing interests

A. Nemudryi and A. Nemudraia are inventors of patents and patent applications related to CRISPR–Cas systems and applications thereof. The other authors declare no competing interests.

Additional information

Extended data is available for this paper at https://doi.org/10.1038/s41564-026-02277-8.

Supplementary information The online version contains supplementary material available at https://doi.org/10.1038/s41564-026-02277-8.

Correspondence and requests for materials should be addressed to Anna Nemudraia or Artem Nemudryi.

Peer review information *Nature Microbiology* thanks the anonymous reviewer(s) for their contribution to the peer review of this work. Peer review reports are available.

https://doi.org/10.1038/s41564-026-02277-8

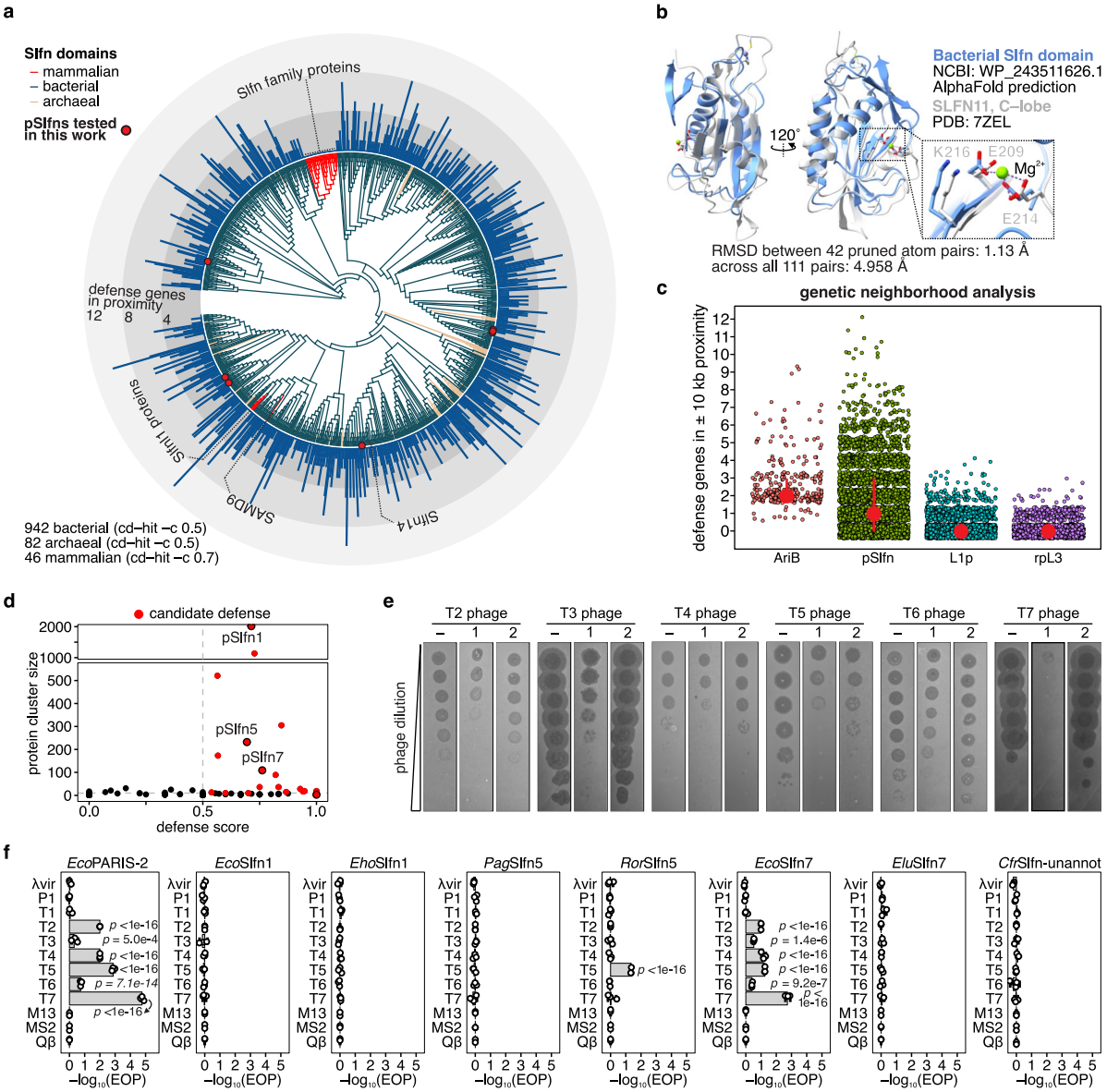

Extended Data Fig. 1 | Prokaryotic Schlafen proteins have anti-phage functions. a, phylogenetic tree of bacterial, archaeal, and mammalian SIfn domains. Tree branches are colored according to the taxonomic group. To improve visualization, the phylogenetic tree was pruned to keep representative sequences identified by CD-HIT from the original dataset. A 50% CD-HIT threshold was used for prokaryotic SIfn domains, while mammalian SIfn domains were pruned with a 70% threshold. Blue bars show the number of phage defense genes in the ±10 kb neighborhood of prokaryotic SIfn genes. **b**, alignment of the AlphaFold predicted structure of the bacterial SIfn domain (light blue) and the C-lobe of the human SLFN11 nuclease domain. The inset shows the ribonuclease active site with amino acid residues required for the catalytic activity. **c**, Scatter plot showing results of genetic neighborhood analysis for AriB (known anti-phage gene), pSIfn, L1p, and rpL3 genes. L1p and rpL3 were used as controls with established non-immune functions. Each dot represents the number of known phage defense genes within a 10 kb neighborhood of AriB, pSIfn, L1p, or rpL3 homologs in our database of prokaryotic genomes. The red dot shows the median value. Vertical red lines show interquartile ranges. **d**, pSIfn proteins were clustered based on domain architectures, annotated using sequence and structural homology methods. Each point represents a pSIfn protein group. *Y-axis:* number of unique sequences in the group; *x-axis*: defense score, which was calculated as the ratio of group members that are found within ± 10 kbp distance from at least one known defense gene to the total number of members in the group (see Methods). Clusters with more than ten representatives (horizontal dashed line) and a defense score > 0.5 (vertical dashed line) were further considered as candidate defense systems (red dots). Black circles show domain architectures experimentally tested in Fig. 1. **e**, A representative phage spot assay showing that *Eco*DUF262-SIfn (1) and *Ror*SIfn5 (2) protect from phages. **f**, Efficiency of plating (EOP) of a panel of *Escherichia coli* phages on MG1655 cells expressing prokaryotic Schlafen proteins. EOP was calculated by dividing plaque-forming units (PFU mL^{-1}) in pSIfn-expressing cells over empty vector control. Data is shown as mean ± SD of three biological replicates. White dots show the average of three technical replicates for each biological replicate. Data were analyzed using one-way Analysis of Variance (ANOVA), and means were compared to the empty vector control using one-sided post-hoc Dunnett's test. The *p* values for statistically significant differences are shown in the plot.

https://doi.org/10.1038/s41564-026-02277-8

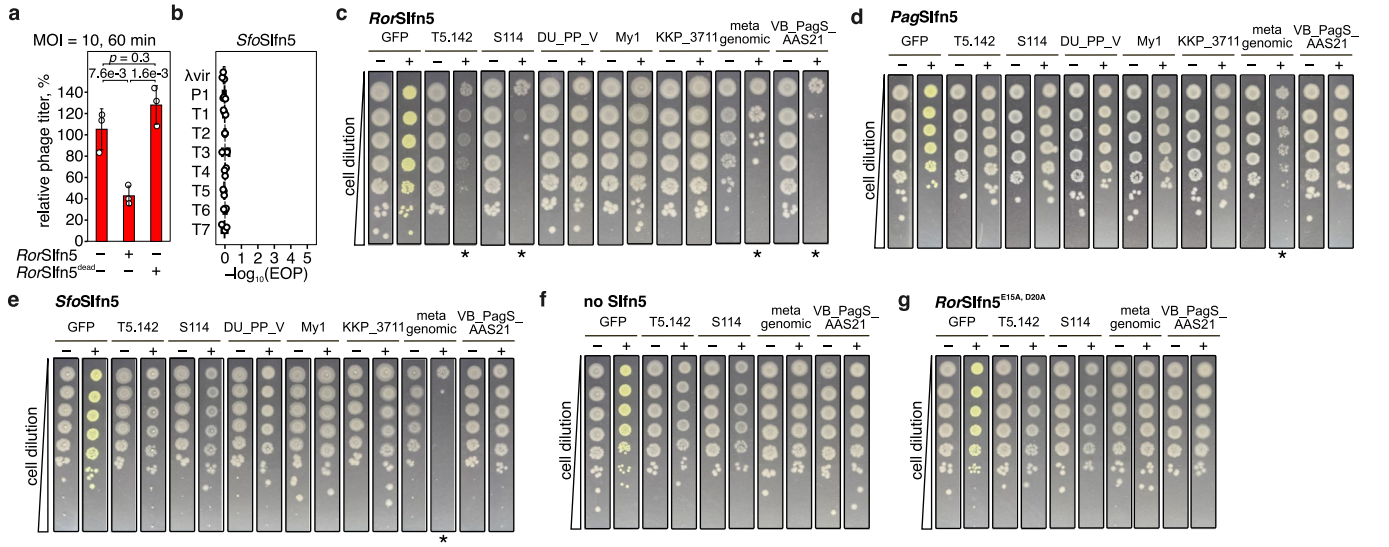

Extended Data Fig. 2 | T5 phage tail assembly protein triggers pSlfn5-mediated phage defense. a, T5 phage titer in supernatants of cells with no defense, *Ror*Slfn5, or catalytic mutant of *Ror*Slfn5 (*Ror*Slfn5^{dead}) was quantified at 50 min post infection with T5 phage at MOI = 10. Phage titers were normalized to the mean of the no-defense control. Data is shown as the mean of three biological replicates ± S.D. One-way ANOVA with post hoc Tukey HSD test was used to compare the experimental groups. The resulting *p* values are shown in the plot. **b**, Antiviral activities of *Sfo*Slfn5 ortholog against a panel of phages. EOP – efficiency of plating. Data is shown as the mean of three biological replicates ± S.D. White dots show the average of three technical replicates for each biological replicate. **c-g**, Cellular toxicity assay in *E. coli* K-12 MG1655 cells co-transformed with a plasmid expressing *Ror*Slfn5 (**c**), *Pag*Slfn5 (**d**), or *Sfo*Slfn5 (**e**) and a plasmid for arabinose-inducible expression of T5.142 homologs (T5.142 – T5 phage, S114 – Salmonella phage S114, DU_PP_V - Pectobacterium phage DU_PP_V, My1 - Pectobacterium phage My1, KKP_3711 - Enterobacter phage KKP_3711, vB_PagS_AAS21 - Pantoea phage vB_PagS_AAS21). Assay was performed in three biological replicates, with one representative replicate shown in the figure. Asterisk (*) indicates toxicity phenotypes. pBAD-GFP was used as a positive control for inducible protein expression. **f-g**, Cellular toxicity assay in MG1655 transformed only with T5.142 homologs (**f**) or co-transformed with a plasmid expressing *Ror*Slfn5^{E15A,D20A} and T5.142 homologs (**g**).

https://doi.org/10.1038/s41564-026-02277-8

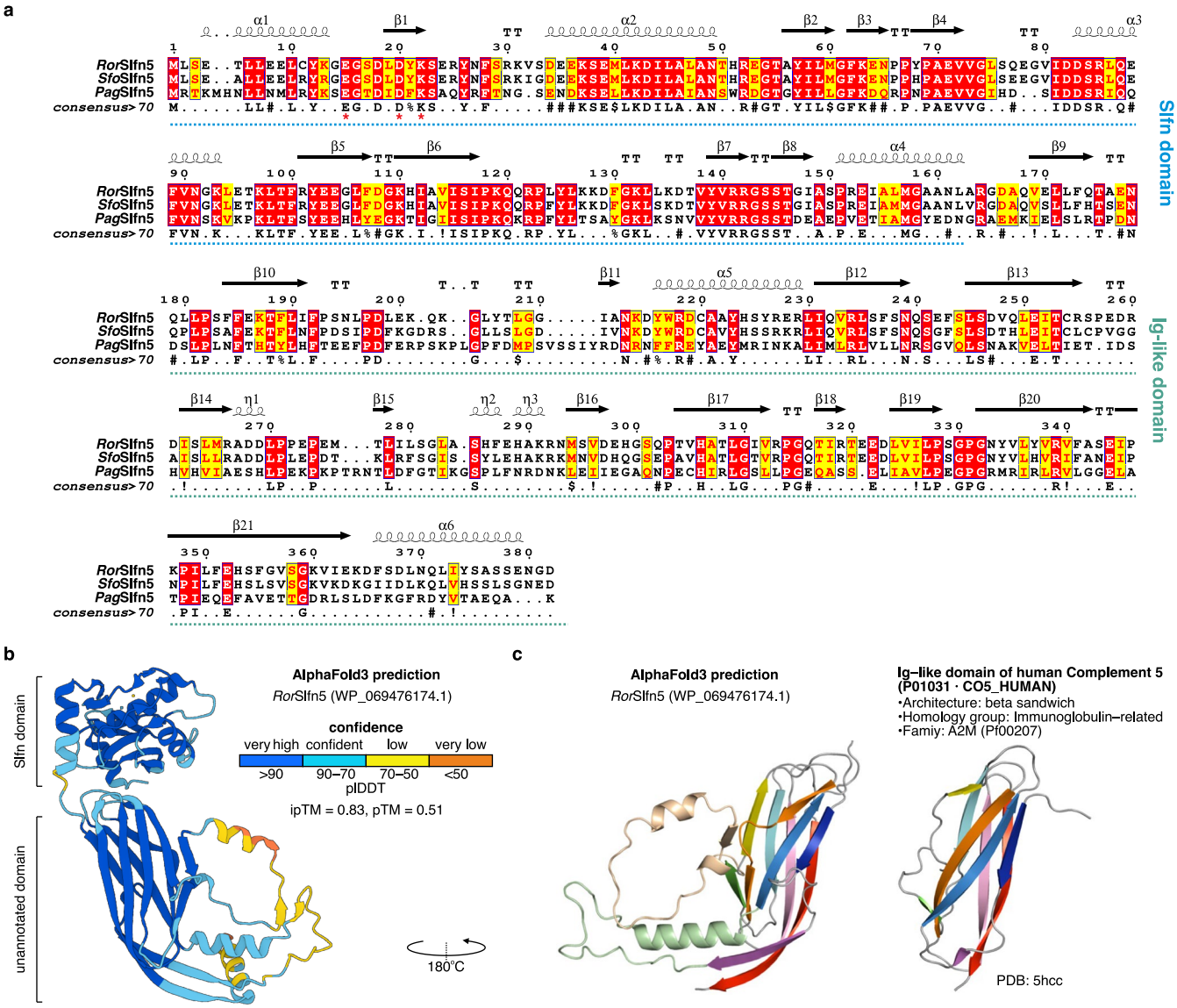

Extended Data Fig. 3 | The C-terminus of pSlfn5 contains an Ig-like phage sensor domain. a, Multiple sequence alignment of pSlfn5 homologs. Red asterisks (*) indicate the conserved catalytic motif of the Slfn ribonuclease domain. **b**, AlphaFold-predicted structure of *Ror*Slfn5. **c**, Comparison of AlphaFold-predicted structures of the C-terminal domain of *Ror*Slfn5 and the Ig-like domain of human Complement 5.

https://doi.org/10.1038/s41564-026-02277-8

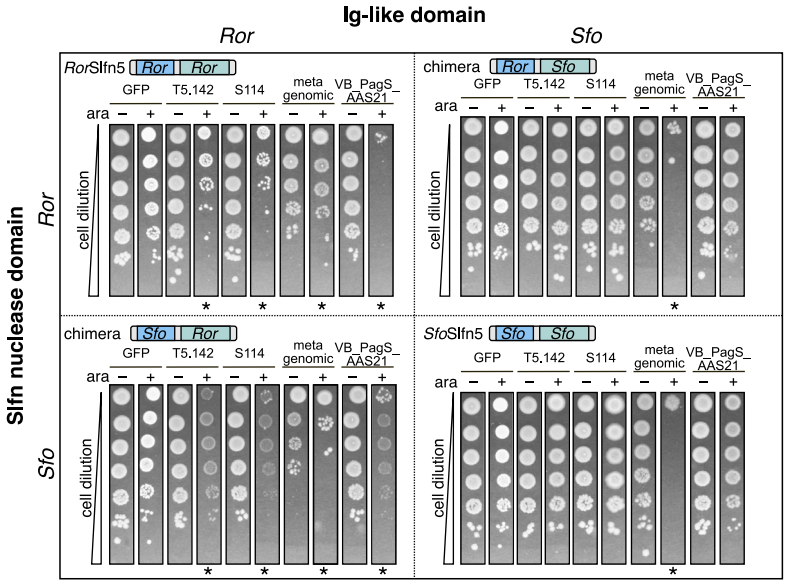

Extended Data Fig. 4 | Ig-like domain of pSlfn5 defense confers phage trigger specificity. Cellular toxicity assay in E. coli K-12 MG1655 cells co-transformed with a plasmid expressing *Ror*Slfn5, *Sfo*Slfn5, or chimeric proteins with swapped Ig-like domains and a plasmid for arabinose-inducible expression of T5.142 homologs (T5.142 – T5 phage, S114 – Salmonella phage S114, DU_PP_V - Pectobacterium phage DU_PP_V, My1 - Pectobacterium phage My1, KKP_3711 - Enterobacter phage KKP_3711, vB_PagS_AAS21 - Pantoea phage vB_PagS_AAS21). Asterisk (*) indicates toxicity phenotypes. pBAD-GFP was used as a positive control for inducible protein expression. Toxicity assays were repeated independently three times with similar results, with data shown for one representative replicate.

https://doi.org/10.1038/s41564-026-02277-8

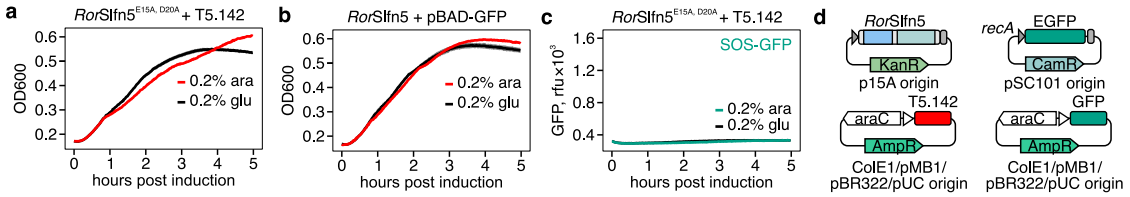

Extended Data Fig. 5 | *Ror*Slfn5 activation does not trigger SOS response. **a**, growth kinetics of MG1655 cells co-transformed with *Ror*Slfn5 and inducible T5.142 plasmid after addition of L-arabinose or D-glucose. **b**, Same for MG1655 co-transformed with *Ror*Slfn5 plasmid and pBAD-GFP. **c**, SOS response reporter assay for MG1655 cells co-transformed with plasmid encoding inactivated *Ror*Slfn5 defense (E15A, D20A mutation). **d**, Schematics of different plasmids used in the SOS response and cell toxicity assays.

https://doi.org/10.1038/s41564-026-02277-8

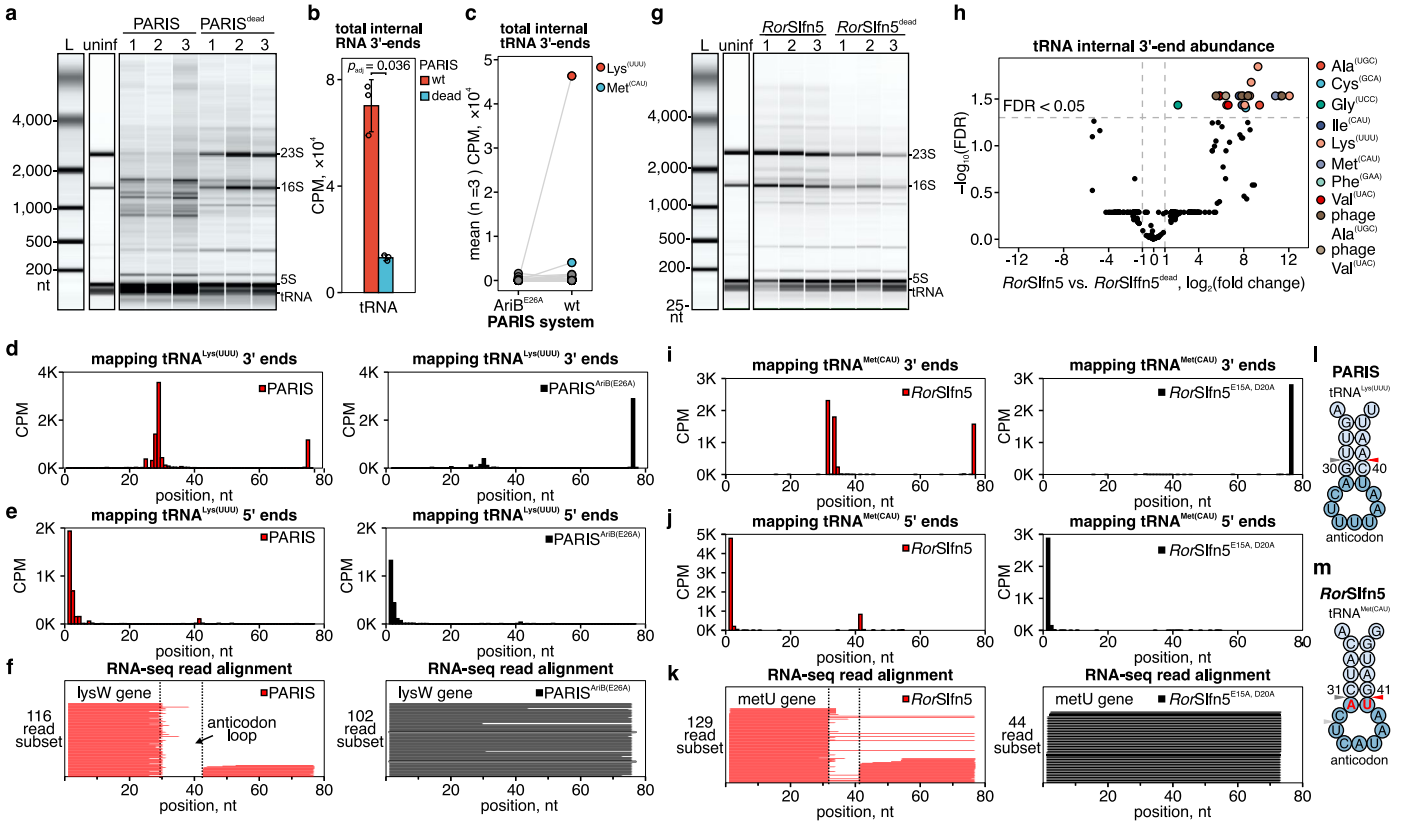

Extended Data Fig. 6 | Phage-activated *Ror*Slfn5 cleaves tRNA anticodon arm. **a**, Agilent 2100 Bioanalyzer gel image for total RNA extracted 30 min post T5 phage infection of MG1655 expressing active PARIS defense or its inactive mutant [PARIS^{dead}; AriB(E26A) mutation]. 1,2,3 – biological replicates. Red asterisks mark phage-associated transcripts absent in the uninfected (uninf) control. **b**, quantification of total 3′-end abundance in tRNA from phage-infected cells expressing PARIS defense vs. PARIS^{dead} control. Data is shown as the mean of three biological replicates ± S.D. Means were compared using a two-sided Welch's t-test. $^{**}p < 0.01$.**c**, quantification of total 3′-ends counts in specific tRNAs. Data is shown as the mean of three biological replicates. **d**-**e**, position-specific mapping of 3′-ends (**d**) and 5′-ends (**e**) in tRNA$^{Lys(UUU)}$ in cells with active (left) or inactive (right) PARIS defense. Data is shown as the mean of three biological replicates. **f**, alignment of sequencing reads to the lysW gene of MG1655 cells in cells with active (left) or inactive (right) PARIS defense. One representative replicate of three biological replicates is shown. **g**, Agilent 2100 Bioanalyzer gel image for total RNA extracted 30 min post T5 phage infection of MG1655 expressing active *Ror*Slfn5 defense or its inactive mutant (*Ror*Slfn$^{E15A, D20A}$). 1,2,3 – biological replicates. Red asterisks mark phage-associated transcripts absent in the uninfected (uninf) control. **h**, position-specific quantification of internal tRNA 3′-ends in cells expressing active vs. inactive *Ror*Slfn5 defense. FDR – false discovery rate. **i-j**, position-specific mapping of 3′-ends (**i**) and 5′-ends (**j**) in tRNA$^{Met(CAU)}$ in cells with active (left) or inactive (right) *Ror*Slfn5 defense. Data is shown as the mean of three biological replicates. **k**, alignment of sequencing reads to the metU gene of MG1655 cells in cells with active (left) or inactive (right) *Ror*Slfn5 defense. One representative replicate of three biological replicates is shown. **l**, position of PARIS nuclease-dependent RNA ends in tRNA$^{Lys(UUU)}$. The red triangle shows the position of mapped internal 5′-ends; the gray triangle shows the position of mapped internal 3′-ends. **m**, same for *Ror*Slfn5 nuclease-dependent RNA ends in tRNA$^{Met(CAU)}$.

https://doi.org/10.1038/s41564-026-02277-8

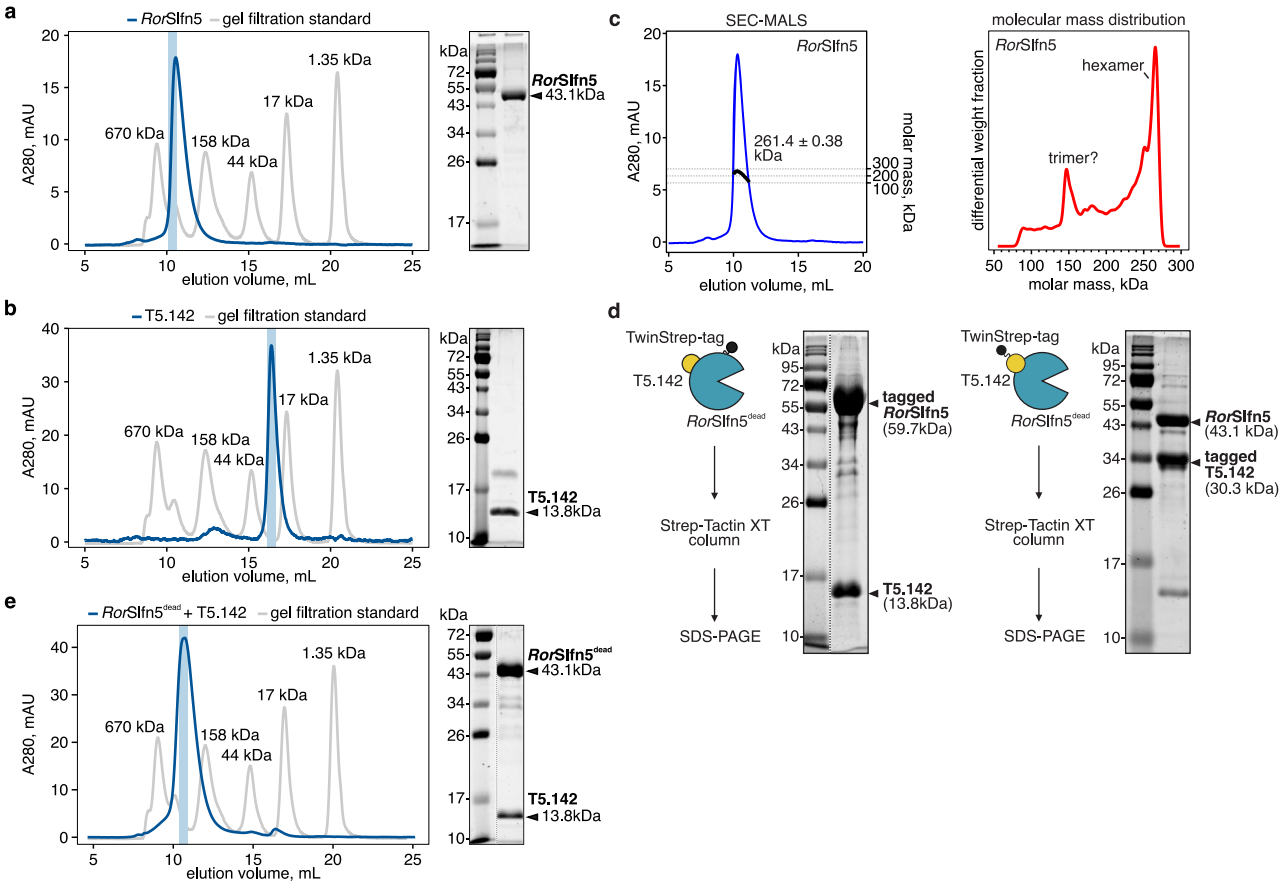

Extended Data Fig. 7 | *Ror*Slfn5 and T5.142 form a stable complex. Size-exclusion chromatography (SEC) profiles of *Ror*Slfn5 (**a**) and T5.142 (**b**) proteins expressed and purified separately. All SEC runs were performed on a Superdex 200 10/300 GL column. Vertical blue rectangles highlight elution fractions used for SDS-PAGE on the right. **c**, SEC with Multi-Angle Static Light Scattering (SEC-MALS) analysis of purified *Ror*Slfn5 protein. **d**, Reciprocal affinity co-purification of *Ror*Slfn5^{dead} and T5.142. *Ror*Slfn5^{dead} (left) or T5.142 (right) protein was tagged with a TwinStrep-6xHis-SUMO tag at the N-terminus (black circle). Proteins were co-expressed, and lysates were applied to the Strep-Tactin XT column. Eluted proteins were visualized with SDS-PAGE followed by protein staining. **e**, Same as in (**a**) and (**b**), but *Ror*Slfn5^{dead} and T5.142 that were co-expressed and co-purified. Experiments shown in (**a**), (**b**), (**d**), and (**e**) were reproduced independently three or more times with similar results.

https://doi.org/10.1038/s41564-026-02277-8

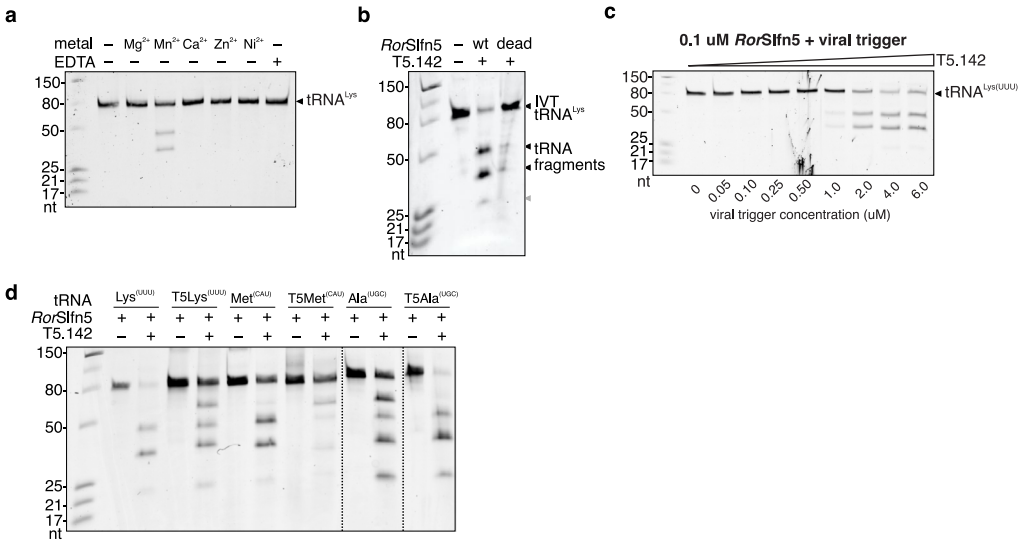

Extended Data Fig. 8 | T5.142 triggers *Ror*Slfn5-mediated tRNA cleavage. **a**, tRNA cleavage assay with 100 nM $tRNA^{Lys(UUU)}$ and 100 nM RorSlfn5 in the presence of trigger T5.142 (2 μM) and 2 mM divalent metals or 2 mM EDTA. RNA fragments were resolved with 15% Urea-PAGE. **b**, tRNA-Lys(UUU) cleavage assay with *Ror*Slfn5 or $RorSlfn5^{E15A, D20A}$ ("dead") in the presence of trigger T5.142 and 2 mM Mn^{2+}. Concentrations of the nuclease, tRNA, and T5.142 are same as in (**a**). **c**, tRNA-Lys(UUU) (100 nM) cleavage assay with *Ror*Slfn5 (100 nM) and varying concentrations of T5.142. Reactions were supplemented with 2 mM Mn^{2+}. **d**, Cleavage assay with varying synthetic tRNAs (100 nM) with 100 nM *Ror*Slfn5 and 2 μM T5.142 in reaction buffer supplemented with 2 mM Mn^{2+}. All shown cleavage assays were reproduced independently three times with similar results.

nature portfolio

Corresponding author(s): Artem Nemudryi, Anna Nemudraia

Last updated by author(s): Jan 13, 2026

Reporting Summary

Nature Portfolio wishes to improve the reproducibility of the work that we publish. This form provides structure for consistency and transparency in reporting. For further information on Nature Portfolio policies, see our Editorial Policies and the Editorial Policy Checklist.

Statistics

For all statistical analyses, confirm that the following items are present in the figure legend, table legend, main text, or Methods section.

n/a	Confirmed	
☐	☒	The exact sample size (*n*) for each experimental group/condition, given as a discrete number and unit of measurement
☐	☒	A statement on whether measurements were taken from distinct samples or whether the same sample was measured repeatedly
☐	☒	The statistical test(s) used AND whether they are one- or two-sided *Only common tests should be described solely by name; describe more complex techniques in the Methods section.*
☒	☐	A description of all covariates tested
☐	☒	A description of any assumptions or corrections, such as tests of normality and adjustment for multiple comparisons
☐	☒	A full description of the statistical parameters including central tendency (e.g. means) or other basic estimates (e.g. regression coefficient) AND variation (e.g. standard deviation) or associated estimates of uncertainty (e.g. confidence intervals)
☐	☒	For null hypothesis testing, the test statistic (e.g. *F*, *t*, *r*) with confidence intervals, effect sizes, degrees of freedom and *P* value noted *Give P values as exact values whenever suitable.*
☒	☐	For Bayesian analysis, information on the choice of priors and Markov chain Monte Carlo settings
☒	☐	For hierarchical and complex designs, identification of the appropriate level for tests and full reporting of outcomes
☒	☐	Estimates of effect sizes (e.g. Cohen's *d*, Pearson's *r*), indicating how they were calculated

Our web collection on statistics for biologists contains articles on many of the points above.

Software and code

Policy information about availability of computer code

Data collection	MinKNOW (v24.11.10) for Nanopore data collection and Dorado Basecaller (v0.9.1) for Nanopore read basecalling; instrument software for SpectraMax M5e (plate reader), Bio-Rad Chemidoc (gel imaging), and Agilent Bioanalyzer (RNA quality).
Data analysis	Homology & Phylogenetics: HMMER (v3.1b2), MAFFT (v7.526), FastTree (v2.1.11), Sequence Alignment: minimap2 (v2.28), Bowtie 2 (v2.5.4), Read Processing & Variant Calling: samtools (v1.21), bcftools (v1.21), bedtools (v2.31.1), cutadapt (v5.0), Protein Structure: AlphaFold 3, DPAM, Statistical Analysis & Visualization: R (v4.3.0) with packages stats and Gviz (v1.44.2); iTOL for tree visualization.

For manuscripts utilizing custom algorithms or software that are central to the research but not yet described in published literature, software must be made available to editors and reviewers. We strongly encourage code deposition in a community repository (e.g. GitHub). See the Nature Portfolio guidelines for submitting code & software for further information.

Data

Policy information about availability of data

All manuscripts must include a data availability statement. This statement should provide the following information, where applicable:

- Accession codes, unique identifiers, or web links for publicly available datasets
- A description of any restrictions on data availability
- For clinical datasets or third party data, please ensure that the statement adheres to our policy

Raw sequencing data were deposited in the NCBI Sequence Read Archive and are publicly available under Bioproject accession numbers PRJNA1272589 (phage genome sequencing) and PRJNA1272590 (3'-end RNA sequencing).

Research involving human participants, their data, or biological material

Policy information about studies with human participants or human data. See also policy information about sex, gender (identity/presentation), and sexual orientation and race, ethnicity and racism.

Reporting on sex and gender	N/A
Reporting on race, ethnicity, or other socially relevant groupings	N/A
Population characteristics	N/A
Recruitment	N/A
Ethics oversight	N/A

Note that full information on the approval of the study protocol must also be provided in the manuscript.

Field-specific reporting

Please select the one below that is the best fit for your research. If you are not sure, read the appropriate sections before making your selection.

☒ Life sciences ☐ Behavioural & social sciences ☐ Ecological, evolutionary & environmental sciences

For a reference copy of the document with all sections, see nature.com/documents/nr-reporting-summary-flat.pdf

Life sciences study design

All studies must disclose on these points even when the disclosure is negative.

Sample size	All experiments were performed in at least three biological replicates which is standard for the field. No sample size calculation was performed.
Data exclusions	No data were excluded from the analyses
Replication	All experiments were performed in at least three biological replicates and successfully reproduced.
Randomization	No randomization was performed.
Blinding	Investigators were not blinded to the group allocation.

Reporting for specific materials, systems and methods

We require information from authors about some types of materials, experimental systems and methods used in many studies. Here, indicate whether each material, system or method listed is relevant to your study. If you are not sure if a list item applies to your research, read the appropriate section before selecting a response.

Materials & experimental systems

n/a	Involved in the study
☒	☐ Antibodies
☒	☐ Eukaryotic cell lines
☒	☐ Palaeontology and archaeology
☒	☐ Animals and other organisms
☒	☐ Clinical data
☒	☐ Dual use research of concern
☒	☐ Plants

Methods

n/a	Involved in the study
☒	☐ ChIP-seq
☒	☐ Flow cytometry
☒	☐ MRI-based neuroimaging

Plants

Seed stocks	N/A
Novel plant genotypes	N/A
Authentication	N/A